Journal of Hydrology X 7 (2020) 100053

Contents lists available at ScienceDirect

Journal of Hydrology X

journal homepage: www.journals.elsevier.com/journal-of-hydrology-x

Research papers

Capture zone models of a multi-well system in aquifers bounded with regular and irregular inflow boundaries

Setareh Nagheli[a], Nozar Samani[a,*], D.A. Barry[b]

[a] Department of Earth Sciences, Shiraz University, Shiraz 7136713565, Iran
[b] Laboratoire de technologie écologique (ECOL), Institut des sciences et technologies de l'environnement (IIE), Faculté de l'environnement naturel, architectural et construit (ENAC), Ecole polytechnique fédérale de Lausanne (EPFL), 1015 Lausanne, Switzerland

ARTICLE INFO

Keywords:
Complex potential
Conformal mapping
Schwarz-Christoffel transformation
Capture zone
Irregular boundaries

ABSTRACT

Being bounded by hydrological (inflow and barrier) boundaries, natural aquifers have regular/irregular shapes. Here, we consider aquifers bounded by segmental inflow (variable head) boundaries in which water is extracted/injected by a multi-well system. Steady state analytical and semi-analytical solutions are derived to delineate the capture envelopes of the multi-well system. The multi-well system includes any number of extraction or injection wells, each with an arbitrary flow rate. The aquifer is bounded by an arbitrary number of boundary segments, with and without uniform regional flow. The solution is fully analytical, and involves hypergeometric functions if the number of boundary segments exceeds three. A sensitivity analysis shows that number, position and extraction/injection rate of wells, numbers and geometry of boundary segments, distance between wells and boundaries, and direction and rate of regional flow independently and collectively control the size, shape and pattern of the capture zones. The derived solutions are useful for sustainable water resources management in terms of both quality and quantity.

1. Introduction

A well capture zone is the volumetric portion of an aquifer from which the well withdraws its water (Intaraprasong and Zhan, 2007; Todd and Mays, 2005). As pumping proceeds, the capture zone grows in size. At steady state, it reaches a maximum size called the capture envelope (Samani and Zarei-Doudeji, 2012). It is affected by pumping rates, hydraulic conductivity, type and configuration of boundaries, and type and position of wells. The delineation of the capture zone in an aquifer-well-stream system plays an important role in the management of surface and subsurface water in terms of both quality and quantity. Javandel and Tsang (1986) presented a series of capture-zone type curves as tools for the design of aquifer clean-up projects. Zarei-Doudeji and Samani (2014) provided capture type curves to design in situ groundwater remediation systems, to contain contaminant plumes, to evaluate surface-groundwater interactions and to verify numerical models. Intaraprasong and Zhan (2007) developed a semi-analytical method to calculate the stream depletion in an aquifer bounded by two parallel streams with and without a streambed. In assessing groundwater-surface water interactions and estimating the stream depletion rate (SDR) due to pumping near a meandering stream, Huang and Yeh (2015) applied the image well method and derived an analytical solution by treating a low-permeability streambed as a Robin condition. They verified the solution with a finite element model and concluded that a meandering stream has a significant effect on SDR compared with a rectilinear geometry. Huang and Yeh (2016) considered a heterogenous confined aquifer with an irregular outer boundary under Dirichlet, Neumann or Robin conditions (or a mix of them) and developed an analytical solution for drawdown. Efforts have also been devoted to quantify the capture time (Zhan and Cao, 2000; Luo and Kitanidis, 2004; Xia et al., 2020).

Capture zone modeling methods may be classified into three model types: analytical, semi-analytical and numerical. Analytical modeling was initiated by Muskat (1946). Bear (1972,1979) extended Muskat's solution for a single fully penetrating well in an infinite confined aquifer with uniform flow using complex velocity potential theory. The approach was generalized to a multi-well system in infinite confined and unconfined aquifers via the superposition principle (Christ and Goltz, 2002; Grubb, 1993; Javandel et al., 1984; Javandel and Tsang, 1986; Shan, 1999; Zhan and Zlotnik, 2002; Zlotnik, 1997). The conjugating image well method (Ferris et al., 1962) with the complex velocity potential as the dependent variable and superposition led to modeling of capture zones in bounded aquifers. Analytical models that predict capture zones include the following cases: single well near an

* Corresponding author.
E-mail address: samanin@shirazu.ac.ir (N. Samani).

https://doi.org/10.1016/j.hydroa.2020.100053
Received 25 November 2019; Received in revised form 2 March 2020; Accepted 9 March 2020
Available online 12 March 2020

Notation

a_j	Coordinate of intersecting points in the ζ plane
b	Aquifer thickness (L)
c	+1 or -1 for extraction and injection wells, respectively
d	Distance between two boundaries (L)
d_D	Dimensionless distance between two boundaries
$_2F_1$	Hypergeometric function
h	Hydraulic head (L)
$\overline{h}_0$	Average of the initial hydraulic head (L)
j	Summation index
K	Hydraulic conductivity (LT^{-1})
l	Aquifer length (L)
N	Number of wells
q_0	Regional uniform flow per unit width (L^2T^{-1})
q_{0D}	Dimensionless regional uniform flow per unit width
Q_w	Pumping or injection rate (L^3T^{-1})
Q_{wD}	Dimensionless pumping or injection rate
Q_{wDj}	Dimensionless pumping or injection rate of the j^{th} well
s	Drawdown (L)
s_D	Dimensionless drawdown
x_{wDj}	Dimensionless x position of the j^{th} well
y_{wDj}	Dimensionless y position of the j^{th} well
z	Complex coordinate in the physical plane
z_{Dsg}	Stagnation point coordinate
z_{wj}	Coordinate of the j^{th} extraction or injection well
z_{wDj}	Dimensionless coordinate of the j^{th} extraction or injection well

Greek

α	Boundaries intersection angle (rad)
β	Angle of the flow direction with the x axis (rad)
δ	Coordinate of the extraction or injection well in the ζ plane
$\overline{\delta}$	Complex conjugate of δ
δ_j	Coordinate of the j^{th} extraction or injection well in the ζ plane
$\delta_j^{'}$	Coordinate of the j^{th} extraction or injection well in the τ plane
ζ	Complex coordinate in the imaginary plane
λ	Ratio of length to width of the aquifer
τ	Complex coordinate in the second imaginary plane
ϕ	Discharge potential and the real part of the complex potential function,Ω (L^3T^{-1})
ϕ_0	Initial potential along the inflow boundary (L^3T^{-1})
ϕ_{0D}	Dimensionless form of ϕ_0
ϕ_D	Dimensionless form of ϕ
ψ	Stream function and imaginary part of the complex potential function, Ω (L^3T^{-1})
ψ_D	Dimensionless ψ
Ω	Complex potential function (L^3T^{-1})
Ω_D	Dimensionless complex potential function

inflow boundary (Strack, 1989; Asadi-Aghbolaghi et al., 2011, 2013), single well between two parallel streams (Intaraprasong and Zhan, 2007), extraction well in a right-angled triangular aquifer (Asadi-Aghbolaghi and Seyyedian, 2010), multi-well system in a wedge-shaped aquifer (Samani and Zarei-Doudeji, 2012), and peninsula-shaped (Zarei-Doudeji and Samani, 2014) and rectangular bounded aquifers (Zarei-Doudeji and Samani, 2018). Conformal mapping is often used instead of the image well method to obtain solutions (Lu et al., 2015; Strack, 1989; Wilson, 1993) since it handles complex boundary conditions, irregularly-shaped aquifers and multiple wells much more conveniently.

For complex situations, semi-analytical and numerical methods are needed, e.g., the capture zone for partially penetrating wells considered by Faybishenko et al. (1995), in which the Range-Kutta method was used. Zlotnik (1997) and Fienen et al. (2005) extended the work of Faybishenko et al. (1995) to the case of an anisotropic aquifer using a similar approach. Schafer (1996) determined the three-dimensional capture zone around horizontal drains and vertical wells by a Range-Kutta particle-tracking algorithm. The capture zone and optimal well spacing of two wells pumping at different flow rates was obtained by Christ and Goltz (2002). They applied the Newton-Raphson method to determine the stagnation point positions.

A range of numerical methods were used for capture zone delineation under different circumstances. For instance, Ahlfeld and Sawyer (1990) described a methodology to determine capture zones for contaminated groundwater remediation. They found well locations and optimal pumping rates under a minimum cost constraint using the finite element method with the optimization handled by a linear programming scheme. Bair and Roadcap (1992) modelled the capture zones of wells in leaky-confined fractured-carbonate aquifers by particle tracking. They used a finite-difference scheme to solve their three-dimensional steady-state flow model, in which they considered five model layers, specified-flux boundary conditions, spatially variable recharge, and recharge from a lake. Capture zones for wells in a stratified-drift buried-valley aquifer were computed by Springer and Bair (1992). Gailey and Gorelick (1993) produced contaminant capture designs under the constraint of minimized pumping rates using the SUTRA model (Voss, 1984). Tiedeman and Gorelick (1993) investigated the uncertainty in optimum extraction rates with a Monte Carlo analysis. The effects of variable density groundwater flow on capture zones were assessed by Taylor and Person (1998) using the finite-element method. A useful tool for numerical modeling of capture zones is MODPATH, which uses the particle-tracking method (Pollock, 1994).

The aim of this research is to obtain analytical/semi-analytical solutions for the capture envelope of a multi-well system in aquifers limited by segmental inflow (variable head) boundaries. The areal extent of the irregularly-shaped aquifer is semi-infinite or finite, solved using complex velocity potentials and conformal mapping. The aquifer system with or without regional groundwater flow includes any number of extraction/injection wells. This paper is organized as follows: Section 2 introduces the conceptual models of investigated aquifers; Section 3 presents a systematic mathematical formulation of the capture zone from simple to complicated boundary conditions; in Section 4 the proposed capture zone models are applied in hypothetical aquifer-well boundary systems and results are discussed. In Section 5 the analytical solutions are validated numerically; Section 6 presents the application of solution in groundwater in situ remediation projects and finally in Section 7 conclusions are summarized.

2. Conceptual model

Aquifers bounded by a stream(s) could have regular or irregular geometries. Fig. 1 gives a schematic plan view of the aquifer-well-boundary systems considered in this paper. The bounding stream can consist of up to n segments and can form finite/semi-infinite shaped aquifers. In semi-infinite cases, aquifers extend to infinity on the unbounded sides. In Fig. 1, the aquifer boundaries are fully penetrating streams (variable head/inflow boundaries) that have no hydraulic resistance with the aquifer. If the uniform regional flow is perpendicular to the inflow boundary, the boundary may be regarded as a constant head boundary. The aquifer is homogeneous and isotropic with uniform thickness. The flow is two dimensional (2-D) and steady. A vertical well

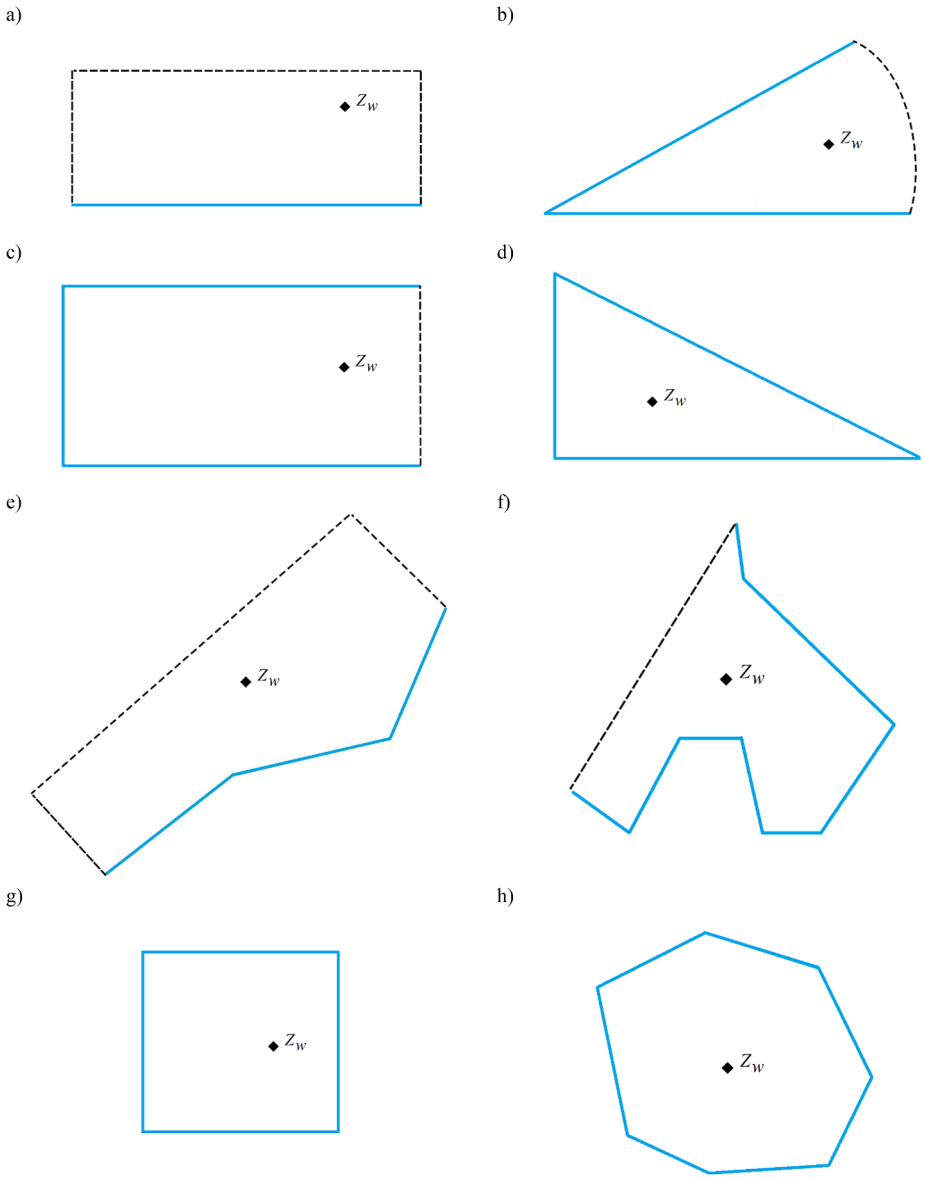

Fig. 1. Schematic plan view of semi-infinite and finite regular and irregular-shaped aquifers. The blue and broken black lines show the inflow and infinite boundaries, respectively. The solid diamond indicates the well location (z_w). (For interpretation of the references to colour in this figure legend, the reader is referred to the web version of this article.)

at z_w fully penetrates the aquifer and is either an extraction or injection well. Although only one well is shown in Fig. 1, the solution derived below is valid for a multiple well system (well field) with or without ambient regional flow (spatially uniform far from the well field), with each well having the same or different extraction/injection rates. The wells can be located anywhere within the aquifer domain.

The simplest bounded aquifer is shown in Fig. 1a. It is a semi-infinite aquifer an inflow boundary (stream/a stream segment) on one side. It extends to infinity in the other sides. Two streams that intersect at angle α form a bounded, wedge-shaped aquifer (Fig. 1b). Streams often meander in plains. If the meander is idealized as a semi-rectangle, it forms a peninsula-shaped aquifer that is bounded by three inflow boundary segments and extends to infinity on the fourth side (Fig. 1c). Coastal aquifers may also be peninsula-shaped. In Fig. 1d, the three stream segments intersect and form a triangular aquifer. More often, the number of boundary segments exceed three and form aquifers of finite or semi-infinite extent. Examples are shown in Fig. 1e–h.

3. Mathematical formulation of the multi-well capture zones

3.1. Case 1: Aquifer bounded with one stream segment

The aquifer of Fig. 1a is first considered that is limited in one side by an inflow boundary (a stream or a segment of a stream), extended to infinity in the other sides and extracted by a well. Using the image well method and due to the linearity of the Laplace equation the complex discharge potential for such a system is written as (Strack, 1989):

$$\Omega(z) = \phi_0 + \frac{Q_w}{2\pi}\left[\ln\left(\frac{z - z_w}{z - \overline{z}_w}\right)\right] \quad (1)$$

where ϕ_0 is the initial potential in the absence of extraction and regional flow, Q_w and z_w denote, respectively, the extraction rate and well position in the complex plane (z), and $\overline{z}_w$ is the complex conjugate of z_w.

Eq. (1) may be rewritten for a multi-well system in the presence of (uniform) regional flow, q_0 [L^2 T^{-1}], at an arbitrary direction β (radians) relative to the positive direction of the x axis (Nagheli et al.,

2020):

$$\Omega(z) = \phi_0 - q_0 z\exp(-i\beta) + \sum_{j=1}^{N} c_j \frac{Q_{wj}}{2\pi}\left[\ln\left(\frac{z - z_{wj}}{z - \overline{z}_{wj}}\right)\right] \quad (2)$$

where i is the complex root, N is the number of wells and j is the summation index. The constant c is $+1$ for extraction wells and -1 for injection wells.

Introducing the following dimensionless (normalized) parameters:

$$z_D = \frac{z}{l},\ z_{wDj} = \frac{z_{wj}}{l},\ Q_{wDj} = \frac{Q_{wj}}{Kbl},$$
$$q_{0D} = \frac{q_0}{Kb},\ \Omega_D(z) = \frac{\Omega(z)}{Kbl} \quad (3)$$

where, K is hydraulic conductivity, and b and l are the aquifer thickness and length of the boundary segment, respectively, Eq. (2) becomes:

$$\Omega_D = \phi_{0D} - q_{0D} z_D\exp(-i\beta) + \sum_{j=1}^{N} c_j \frac{Q_{wDj}}{2\pi}\left[\ln\left(\frac{z_D - z_{wDj}}{z_D - \overline{z}_{wDj}}\right)\right] \quad (4)$$

The real and the imaginary components of Ω_D, are the dimensionless discharge potential and stream function, respectively.

$$\phi_D = \phi_{0D} - q_{0D}(x_D\cos\beta + y_D\sin\beta) + \sum_{j=1}^{N} c_j \frac{Q_{wDj}}{4\pi}\left\{\ln\left[\frac{(x_D - x_{wD})^2 + (y_D - y_{wD})^2}{(x_D - x_{wD})^2 + (y_D + y_{wD})^2}\right]\right\} \quad (5)$$

$$\psi_D = -q_{0D}(y_D\cos\beta - x_D\sin\beta) + \sum_{j=1}^{N} c_j \frac{Q_{wDj}}{2\pi}\left[\tan^{-1}\left(\frac{y_D - y_{wD}}{x_D - x_{wD}}\right) - \tan^{-1}\left(\frac{y_D + y_{wD}}{x_D - x_{wD}}\right)\right] \quad (6)$$

A stagnation point exists where the flow velocity is zero. A streamline passing through a stagnation point forms the capture envelope and separates the regions of flow. The positions of stagnation points are defined where the gradient of the complex potential (Eq. (4)) vanishes:

$$\frac{d\Omega_D}{dz_D} = \sum_{j=1}^{N} c_j \frac{Q_{wj}}{2\pi}\left[\frac{1}{z_D - z_{wDj}} - \frac{1}{z_D - \overline{z}_{wDj}}\right] - q_{0D}\exp(-i\beta) = 0 \quad (7)$$

The roots of Eq. (7) define the position of stagnation points (z_{Dsg}). For a single well, the positive root can be calculated analytically as:

$$z_{Dsg} = \frac{1}{2}\left\{\left[({z_{wD}}^2 - 2z_{wD}\overline{z}_{wD} + {\overline{z}_{wD}}^2) + \frac{4(z_{wD} - \overline{z}_{wD})}{q_{0D}exp(-i\beta)}\right]^{\frac{1}{2}} + z_{wD} + \overline{z}_{wD}\right\} \quad (8)$$

For the multiple-well systems the roots of Eq. (7) are determined numerically. Plotting Eqs. (5), (6) and (8) results in the capture zone consisting of equipotential lines and streamlines.

3.2. Case 2: Aquifers bounded with two stream segments

The aquifer of Fig. 1b is limited by two inflow boundaries or two segments of an inflow boundary intersecting or connecting each other at an angle (α) and forming a wedge-shaped aquifer. The solutions of Samani and Zarei-Doudeji (2012) for wedge-shaped aquifers are limited to the case of α being a multiple of π. If α is too low, the number of image wells becomes large, making the solution cumbersome. Therefore, the application of image well method is not recommended in this case. A better approach is to map the model from the physical plane (z) onto a simpler plane (ζ) (Fig. 2) based on the Schwarz-Christoffel transformation (Driscoll and Trefethen, 2002). The origin of the x-y axes is located at point 2. In the ζ-plane, the ξ axis is the horizontal axis and the η axis is perpendicular to it at point 2. Based on the Schwarz-Christoffel transformation, the relation between z and ζ is (Strack, 1989):

$$z(\zeta) = C_1 \int \zeta^{\frac{\alpha}{\pi}-1} d\zeta + C_2 \quad (9)$$

where, $z = x + iy$, $\zeta = \xi + i\eta$ and C_1 and C_2 are constants. Substituting the positions of points 2 and z_w in the z and ζ- planes into Eq. (9) gives the z and ζ values as (see also Table 1)

$$\frac{z}{|z_w|} = \zeta^{\frac{\alpha}{\pi}} \quad (10)$$

Or

$$\zeta = \left[\frac{z}{|z_w|}\right]^{\frac{\pi}{\alpha}} \quad (11)$$

The complex discharge potential in a wedge-shaped aquifer for a well in the ζ-plane is (Strack, 1989):

$$\Omega(\zeta) = \phi_0 + \frac{Q_w}{2\pi}\left[\ln\left(\frac{\zeta - \delta}{\zeta - \overline{\delta}}\right)\right] \quad (12)$$

where δ is the position of the well in the ζ-plane and $\overline{\delta}$ is the complex conjugate of δ.

Applying the superposition principle, Eq. (12) may be extended for a multi-well system in a wedged-shaped aquifer with a uniform regional flow as:

$$\Omega(\zeta) = \phi_0 - q_0\zeta^{\frac{\alpha}{\pi}}|z_w|\exp(-i\beta) + \sum_{j=1}^{N} c_j \frac{Q_{wj}}{2\pi}\left[\ln\left(\frac{\zeta - \delta_j}{\zeta - \overline{\delta_j}}\right)\right] \quad (13)$$

Based on Eq. (11), Eq. (13) is transformed to the z-plane:

$$\Omega(z) = \phi_0 - q_0 z\exp(-i\beta) + \sum_{j=1}^{N} c_j \frac{Q_{wj}}{2\pi}\left\{ln\left[\frac{\left(\frac{z}{|z_{wj}|}\right)^{\frac{\pi}{\alpha}} - \left(\frac{z_{wj}}{|z_{wj}|}\right)^{\frac{\pi}{\alpha}}}{\left(\frac{z}{|z_{wj}|}\right)^{\frac{\pi}{\alpha}} - \left(\frac{\overline{z}_{wj}}{|z_{wj}|}\right)^{\frac{\pi}{\alpha}}}\right]\right\} \quad (14)$$

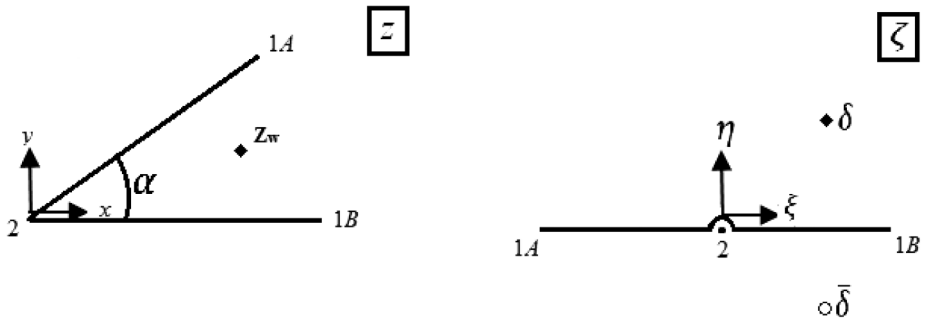

Fig. 2. Mapping the wedge-shaped aquifer from the physical plane (z) to the imaginary plane (ζ). Solid diamonds are locations of the real wells. Hollow circles illustrate image wells of the opposite type to the real well.δ shows the spatial location of the extraction or injection well in the ζ plane and $\overline{\delta}$ is complex conjugate of δ.

Table 1
Schwarz-Christoffel transformation for each aquifer type.

Number of aquifer boundary segments	Aquifer type	Schwarz-Christoffel transformation
One (Fig. 1a)	Semi-infinite aquifer	$\zeta = z$
Two (Fig. 2)	Wedge-shaped aquifer	$\zeta = \left[\frac{z}{\lvert z_w \rvert}\right]^{\frac{\pi}{\alpha}}$
Three (Fig. 3)	Peninsula-shaped aquifer	$\zeta = \sinh^2\left(\frac{\pi z}{d}\right)$
	Triangular aquifer Semi-infinite aquifer	$z = m\zeta^{\frac{\alpha_2}{\pi}}\left(\frac{2F1\left(\frac{-\alpha_1}{\pi}+1, \frac{\alpha_2}{\pi}; \frac{\alpha_2}{\pi}+1; -\zeta\right)}{\frac{\alpha_2}{\pi}}\right) = M(\zeta)$
		$\zeta = M^{-1}(z)$
Four (Fig. 5)	Rectangular aquifer	$z = \frac{\lambda d}{K(m)}\int \frac{d\tau}{\sqrt{(1-\tau^2)(1-m\tau^2)}}$
		$\tau = sn\left(\frac{zK(m)}{\lambda d}\right)$
		$= \frac{sn\left(\frac{xK(m)}{\lambda d}\right)\overline{dn}\left(\frac{yK(m)}{\lambda d}\right) + icn\left(\frac{xK(m)}{\lambda d}\right)dn\left(\frac{xK(m)}{\lambda d}\right)\overline{sn}\left(\frac{yK(m)}{\lambda d}\right)\overline{cn}\left(\frac{yK(m)}{\lambda d}\right)}{\overline{cn}^2\left(\frac{yK(m)}{\lambda d}\right) + msn^2\left(\frac{xK(m)}{\lambda d}\right)\overline{sn}^2\left(\frac{yK(m)}{\lambda d}\right)}$
		$= Re^{i\theta}$
Four or more (Fig. 4)	Semi-finite/finite regularly- or irregularly-shaped aquifer	$z = C_1\int\prod_{j=1}^{N-1}(\zeta - a_j)^{\alpha_j - 1}d\zeta + C_2$, Numerical solution

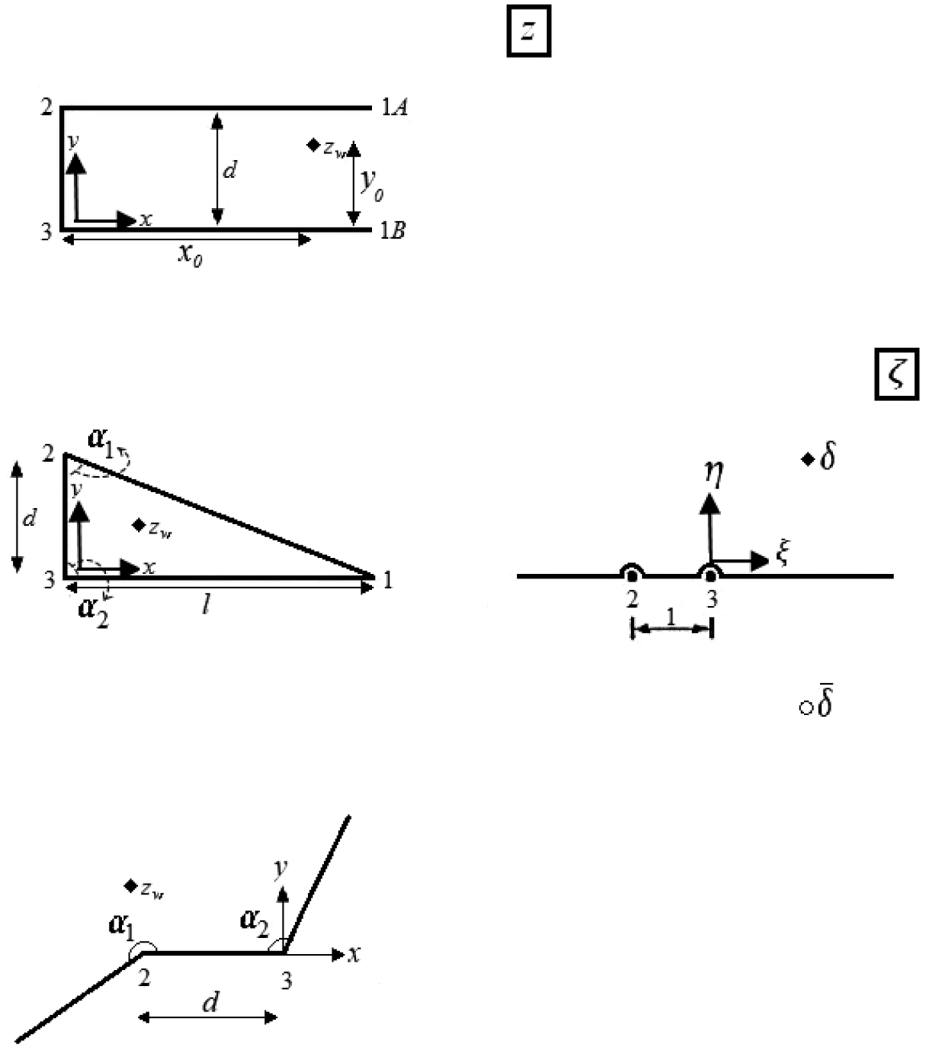

Fig. 3. Mapping the aquifers with three boundary segments from the physical plane (z) to the ζ plane. Solid diamonds show position of the real wells. Hollow circles indicate image wells of the opposite type to the real well.δ shows the spatial location of the extraction or injection well in the ζ plane and $\overline{\delta}$ is complex conjugate of δ.

Using the following dimensionless parameters:

$$z_D = \frac{z}{r},\ z_{wDj} = \frac{z_{wj}}{r},\ Q_{wDj} = \frac{Q_{wj}}{Kbr},$$
$$q_{0D} = \frac{q_0}{Kb},\ \Omega_D(z) = \frac{\Omega(z)}{Kbr} \tag{15}$$

where r is the radius of the wedge, Eq. (14) becomes:

$$\Omega_D = \phi_{0D} - q_{0D} z_D \exp(-i\beta) + \sum_{j=1}^{N} c_j \frac{Q_{wDj}}{2\pi} \left\{ ln \left[\frac{\left(\frac{z_D}{|z_{wDj}|}\right)^{\frac{\pi}{\alpha}} - \left(\frac{z_{wDj}}{|z_{wDj}|}\right)^{\frac{\pi}{\alpha}}}{\left(\frac{z_D}{|z_{wDj}|}\right)^{\frac{\pi}{\alpha}} - \left(\frac{\bar{z}_{wDj}}{|z_{wDj}|}\right)^{\frac{\pi}{\alpha}}} \right] \right\} \tag{16}$$

Substituting $r_D(\cos\theta + i\sin\theta)$ for z_D, the dimensionless discharge potential is given by the real part of Eq. (16):

$$\phi_D = \phi_{0D} - q_{0D} r_D \cos(\theta + \beta) + \sum_{j=1}^{N} c_j \frac{Q_{wDj}}{4\pi} \times$$
$$\left\{ \ln \left[\frac{\left[\left(\frac{1}{r_{wDj}}\right)^{\frac{\pi}{\alpha}} \cos\left(\frac{\pi\theta}{\alpha}\right) - \cos\left(\frac{\pi\theta_w}{\alpha}\right)\right]^2 + \left[\left(\frac{1}{r_{wDj}}\right)^{\frac{\pi}{\alpha}} \sin\left(\frac{\pi\theta}{\alpha}\right) - \sin\left(\frac{\pi\theta_w}{\alpha}\right)\right]^2}{\left[\left(\frac{1}{r_{wDj}}\right)^{\frac{\pi}{\alpha}} \cos\left(\frac{\pi\theta}{\alpha}\right) - \cos\left(\frac{\pi\theta_w}{\alpha}\right)\right]^2 + \left[\left(\frac{1}{r_{wDj}}\right)^{\frac{\pi}{\alpha}} \sin\left(\frac{\pi\theta}{\alpha}\right) + \sin\left(\frac{\pi\theta_w}{\alpha}\right)\right]^2} \right] \right\} \tag{17}$$

The imaginary part of Eq. (16) is the stream function:

$$\psi_D = -q_{0D} r_D \sin(\theta - \beta) + \sum_{j=1}^{N} c_j \frac{Q_{wDj}}{2\pi} \times$$
$$\left\{ \tan^{-1}\left(\frac{\left(\frac{1}{r_{wDj}}\right)^{\frac{\pi}{\alpha}} \sin\left(\frac{\pi\theta}{\alpha}\right) - \sin\left(\frac{\pi\theta_w}{\alpha}\right)}{\left[\frac{1}{r_{wDj}}\right]^{\frac{\pi}{\alpha}} \cos\left(\frac{\pi\theta}{\alpha}\right) - \cos\left(\frac{\pi\theta_w}{\alpha}\right)} \right) - \tan^{-1}\left(\frac{\left[\frac{1}{r_{wDj}}\right]^{\frac{\pi}{\alpha}} \sin\left(\frac{\pi\theta}{\alpha}\right) + \sin\left(\frac{\pi\theta_w}{\alpha}\right)}{\left[\frac{1}{r_{wDj}}\right]^{\frac{\pi}{\alpha}} \cos\left(\frac{\pi\theta}{\alpha}\right) - \cos\left(\frac{\pi\theta_w}{\alpha}\right)} \right) \right\} \tag{18}$$

Calculating the derivative of Eq. (16) and setting it to zero gives the coordinates of stagnation points:

$$\frac{d\Omega_D}{dz_D} = -q_{0D} \exp(-i\beta)$$
$$+ \sum_{j=1}^{N} c_j \frac{Q_{wDj}}{2\pi} \left[\frac{\pi z_D^{\frac{\pi}{\alpha}-1}}{\alpha\left(z_D^{\frac{\pi}{\alpha}} - z_{wDj}^{\frac{\pi}{\alpha}}\right)} - \frac{\pi z_D^{\frac{\pi}{\alpha}-1}}{\alpha\left(z_D^{\frac{\pi}{\alpha}} - \bar{z}_{wDj}^{\frac{\pi}{\alpha}}\right)} \right] = 0 \tag{19}$$

As mentioned above, equations of the discharge potential (Eq. (17)), stream function (Eq. (18)) and the stagnation points (Eq. (19)) are solved and plotted to delineate the capture zones.

3.3. Case 3: aquifers bounded with three stream segments

The aquifers of Fig. 1c–e are surrounded by three inflow (variable head) boundary segments. To derive the capture zone equations, the aquifers are transformed from the z-plane to the upper half ζ-plane (Fig. 3) using the Schwarz-Christoffel transformation. After transformation, the coordinates of points 1–3 in the ζ-plane are: $\zeta_1 = \infty$, $\zeta_2 = -1$ and $\zeta_3 = 0$. The Schwarz-Christoffel transformation for these aquifers is:

$$z(\zeta) = C_1 \int (\zeta + 1)^{\frac{\alpha_1}{\pi}-1} \zeta^{\frac{\alpha_2}{\pi}-1} d\zeta + C_2 \tag{20}$$

where, C_1 and C_2 are constants that control the size of figures and the location of origin in the z-plane, respectively. C_2 equals to zero because $z = 0$ corresponds to $\zeta = 0$.

Case 3a: For the case of peninsula-shaped aquifer (Fig. 1c), $\alpha_1 = \alpha_2 = \pi/2$ and Eq. (20) is rewritten as:

$$z(\zeta) = C_1 \int (\zeta + 1)^{\frac{-1}{2}} \zeta^{\frac{-1}{2}} d\zeta + C_2 \tag{21}$$

At points 3 and 2, $\zeta = 0$ and $\zeta = -1$, respectively, so $C_1 = d/\pi$ and $C_2 = 0$. Therefore, the relation between z and ζ is:

$$z = \frac{d}{\pi} \ln\left[(\zeta + 1)^{\frac{1}{2}} + \zeta^{\frac{1}{2}} \right] \tag{22}$$

or

$$\zeta = \sinh^2\left(\frac{\pi z}{d}\right) \tag{23}$$

where, d is the aquifer width (Table 1).

The complex potential for a multi-well system in this aquifer is obtained in the ζ-plane by the application of the image well method and the superposition principle:

$$\Omega(\zeta) = \phi_0 - \frac{dq_0}{\pi} \ln(\sqrt{\zeta + 1} + \sqrt{\zeta}) \exp(-i\beta) + \sum_{j=1}^{N} c_j \frac{Q_{wj}}{2\pi} \left[\ln\left(\frac{\zeta - \delta_j}{\zeta - \bar{\delta}_j} \right) \right] \tag{24}$$

Based on Eq. (23), Eq. (24) can be rewritten in terms of z as:

$$\Omega(z) = \phi_0 - q_0 z \exp(-i\beta) + \sum_{j=1}^{N} c_j \frac{Q_{wj}}{2\pi} \left\{ ln \left[\frac{sinh^2\left(\frac{\pi z}{d}\right) - sinh^2\left(\frac{\pi z_{wj}}{d}\right)}{sinh^2\left(\frac{\pi z}{d}\right) - sinh^2\left(\frac{\pi \bar{z}_{wj}}{d}\right)} \right] \right\} \tag{25}$$

Using the following dimensionless parameters:

$$z_D = \frac{z}{d},\ z_{wDj} = \frac{z_{wj}}{d},\ Q_{wDj} = \frac{Q_{wj}}{Kbd},\ q_{0D} = \frac{q_0}{Kb},$$
$$\Omega_D(z) = \frac{\Omega(z)}{Kbd},\ x_D = \frac{x}{d},\ y_D = \frac{y}{d} \tag{26}$$

Eq. (25) is generalized as:

$$\Omega_D = \phi_{0D} - q_{0D} z_D \exp(-i\beta)$$
$$+ \sum_{j=1}^{N} c_j \frac{Q_{wDj}}{2\pi} \left[\ln\left(\frac{\sinh^2(\pi z_D) - \sinh^2(\pi z_{wDj})}{\sinh^2(\pi z_D) - \sinh^2(\pi \bar{z}_{wDj})} \right) \right] \tag{27}$$

The real part of Eq. (27) gives the dimensionless potential:

$$\phi_D = \phi_{0D} - q_{0D}(x_D \cos\beta + y_D \sin\beta)$$
$$+ \sum_{j=1}^{N} c_j \frac{Q_{wDj}}{4\pi} \left\{ \ln\left[\frac{(f_{1D} - f_{2D})^2 + (g_{1D} - g_{2D})^2}{(f_{1D} - f_{2D})^2 + (g_{1D} + g_{2D})^2} \right] \right\} \tag{28}$$

while the imaginary part gives the dimensionless stream function:

$$\psi_D = -q_{0D}(y_D \cos\beta - x_D \sin\beta)$$
$$+ \sum_{j=1}^{N} c_j \frac{Q_{wDj}}{2\pi} \left[\tan^{-1}\left(\frac{g_{1D} - g_{2D}}{f_{1D} - f_{2D}} \right) - \tan^{-1}\left(\frac{g_{1D} + g_{2D}}{f_{1D} - f_{2D}} \right) \right] \tag{29}$$

where f_{1D}, f_{2D}, g_{1D} and $g_{2D}$are given in Appendix A. The roots of the first derivative of Eq. (27) give the stagnation points:

$$\frac{d\Omega_D}{dz_D} = -q_{0D} \exp(-i\beta) +$$
$$\sum_{j=1}^{N} c_j \frac{Q_{wDj}}{2\pi} \left[\frac{2\pi sinh(\pi z_D) cosh(\pi z_D)}{sinh^2(\pi z_D) - sinh^2(\pi z_{wDj})} - \frac{2\pi sinh(\pi z_D) cosh(\pi z_D)}{sinh^2(\pi z_D) - sinh^2(\pi \bar{z}_{wDj})} \right] = 0 \tag{30}$$

Roots of this equation (coordinates of stagnation points) were calculated numerically in MATLAB.

Case 3b: For the cases of the triangular (Fig. 1d) and the semi-infinite aquifers (Fig. 1e), Eq. (20) equals (Appendix B and Table 1):

$$z = \frac{C_1 \zeta^{\frac{\alpha_2}{\pi}} {}_2F_1\left(\frac{-\alpha_1}{\pi} + 1,\ \frac{\alpha_2}{\pi};\ \frac{\alpha_2}{\pi} + 1;\ -\zeta\right)}{\frac{\alpha_2}{\pi}} \tag{31}$$

where, ${}_2F_1$ is a hypergeometric function. Based on Appendix B, Eq. (31) can be written as:

$$z = m\zeta^{\frac{\alpha_2}{\pi}}\left(\frac{{}_2F_1\left(\frac{-\alpha_1}{\pi}+1,\frac{\alpha_2}{\pi};\frac{\alpha_2}{\pi}+1;-\zeta\right)}{\frac{\alpha_2}{\pi}}\right) = M(\zeta) \tag{32}$$

where m is defined in Eq. (B-2) in Appendix B and

$$\zeta = M^{-1}(z) \tag{33}$$

The complex potential for a multi-well system in these aquifers in the ζ-plane is:

$$\Omega(\zeta) = \phi_0 - q_0 M(\zeta)\exp(-i\beta) + \sum_{j=1}^{N} c_j \frac{Q_{wj}}{2\pi}\ln\left(\frac{\zeta-\delta_j}{\zeta-\overline{\delta_j}}\right) \tag{34}$$

Eq. (34) can be rewritten in terms of z using Eq. (33):

$$\Omega(z) = \phi_0 - q_0 z\exp(-i\beta) + \sum_{j=1}^{N} c_j \frac{Q_{wj}}{2\pi}\left[\ln\left(\frac{M^{-1}(z)-M^{-1}(z_w)}{M^{-1}(z)-M^{-1}(\overline{z}_w)}\right)\right] \tag{35}$$

Using the following dimensionless parameters:

$$z_D = \frac{z}{d},\ z_{wDj} = \frac{z_{wj}}{d},\ Q_{wDj} = \frac{Q_{wj}}{Kbd},$$
$$q_{0D} = \frac{q_0}{Kb},\ \Omega_D(z) = \frac{\Omega(z)}{Kbd} \tag{36}$$

Eq. (35) is rewritten as:

$$\Omega_D = \phi_{0D} - q_{0D} z_D\exp(-i\beta) + \sum_{j=1}^{N} c_j \frac{Q_{wDj}}{2\pi}\left[\ln\left(\frac{M^{-1}(z_D)-M^{-1}(z_{wD})}{M^{-1}(z_D)-M^{-1}(\overline{z}_{wD})}\right)\right] \tag{37}$$

Setting the real part and the imaginary part of M^{-1} equal to U and V, respectively, the real part of Eq. (37) is the dimensionless discharge potential and the imaginary part equals the dimensionless stream function as follows:

$$\phi_D = \phi_{0D} - q_{0D}(x_D\cos\beta + y_D\sin\beta) + \sum_{j=1}^{N} c_j \frac{Q_{wDj}}{4\pi}\left\{\ln\left[\frac{(U_D-U_{wD})^2+(V_D-V_{wD})^2}{(U_D-U_{wD})^2+(V_D+V_{wD})^2}\right]\right\} \tag{38}$$

and

$$\psi_D = -q_{0D}(y_D\cos\beta - x_D\sin\beta) + \sum_{j=1}^{N} c_j \frac{Q_{wDj}}{2\pi}\left[\tan^{-1}\left(\frac{V_D-V_{wD}}{U_D-U_{wD}}\right) - \tan^{-1}\left(\frac{V_D+V_{wD}}{U_D-U_{wD}}\right)\right] \tag{39}$$

The stagnation points computed using Eq. (34) are:

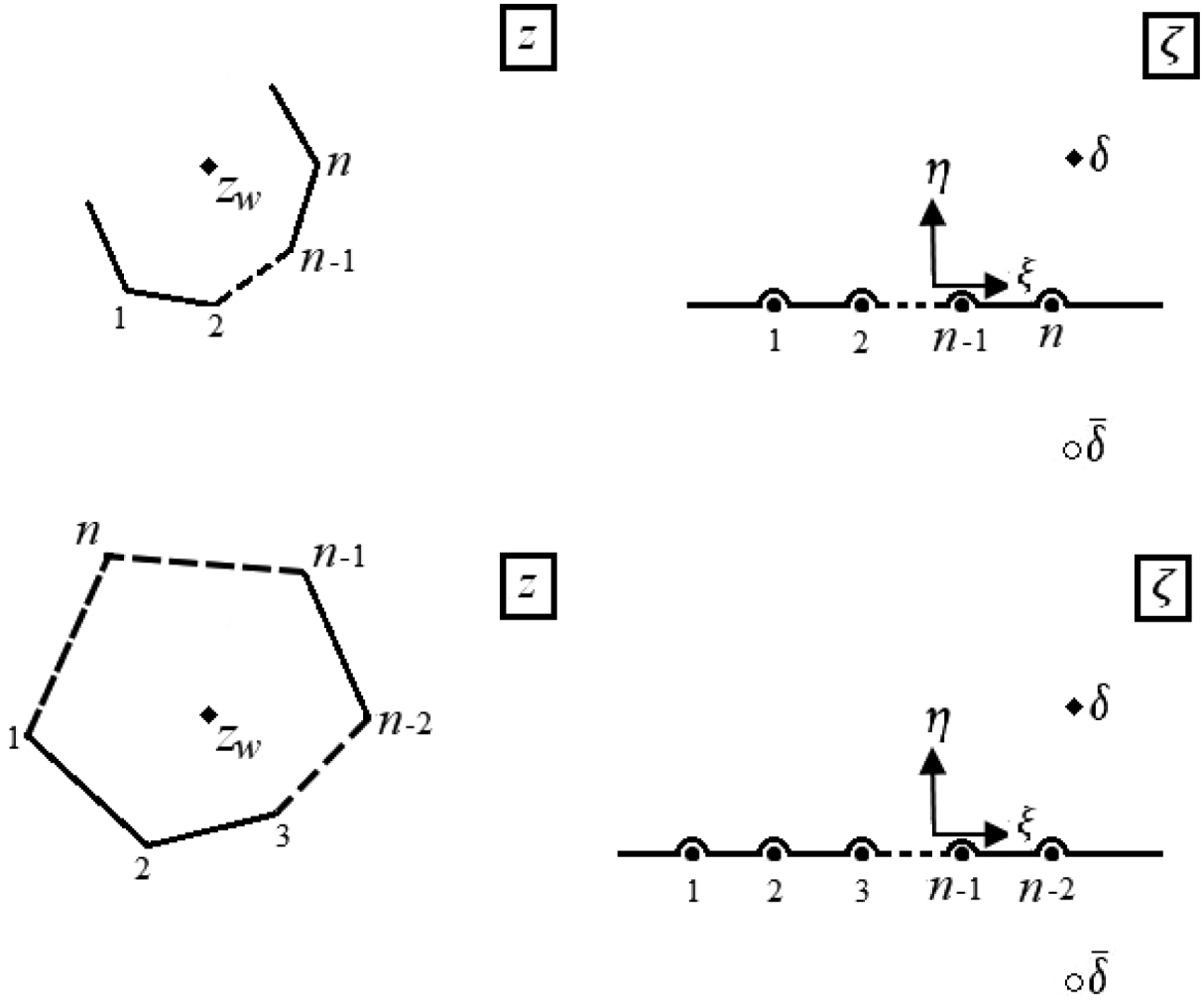

Fig. 4. Mapping the semi-finite and finite aquifers from the physical plane (z) to the imaginary plane (ζ). Solid diamonds and the hollow circles illustrate position of the real wells and image wells of the opposite type to the real well, respectively.δ indicate the position of the extraction or injection wells in the ζ plane and $\overline{\delta}$ is complex conjugate of δ.

$$\frac{d\Omega(\zeta)}{d\zeta} = -q_{0D}\exp(-i\beta)m\zeta^{\frac{\alpha_2}{\pi}-1}\,{}_2F_1\left(\frac{-\alpha_1}{\pi}+1,\ \frac{\alpha_2}{\pi};\ \frac{\alpha_2}{\pi}+1;\ -\zeta\right) - \frac{q_{0D}\exp(-i\beta)m\zeta^{\frac{\alpha_2}{\pi}-1}\left(\frac{\alpha_1}{\pi}+1\right){}_2F_1\left(\frac{-\alpha_1}{\pi}+2,\frac{\alpha_2}{\pi}+1;\frac{\alpha_2}{\pi}+2;-\zeta\right)}{\frac{\alpha_2}{\pi}+1} + \sum_{j=1}^{N} c_j\frac{Q_{wj}}{2\pi}\left[\frac{1}{\zeta-\delta_j}-\frac{1}{\zeta-\delta_j}\right] = 0 \tag{40}$$

Eq. (40) is solved numerically using MATLAB, with the stagnation points in the z-plane determined with Eq. (33).

3.4. Case 4: Aquifers bounded with four or more stream segments

The number of boundary segments for the rectangular/polygonal-shaped aquifers of Fig. 1f–h is greater than three, while the aquifers may have finite or semi-finite extent. To model their capture zones, the aquifers of Fig. 1f–h are mapped from the z-plane onto the ζ-plane using the Schwarz-Christoffel transformation (Fig. 4).

The Schwarz-Christoffel transformation for these aquifers is:

$$z = C_1\int\prod_{j=1}^{N-1}(\zeta-a_j)^{\alpha_j-1}d\zeta + C_2 \tag{41}$$

where, a is prevertex position in the ζ-plane, α equals angle between boundaries in radian and N is number of vertices.

Case 4a: When the rectangular aquifer is transformed from the z-plane to the upper half of the ζ-plane (Fig. 5), the coordinates of points 1–4 in the ζ -plane are: $\zeta_1 = \infty$, $\zeta_2 = 0$, $\zeta_3 = 1$ and $\zeta_4 = 1/m$ while $\alpha_1 = \alpha_2 = \alpha_3 = \alpha_4 = \pi/2$, so Eq. (41) can be written as (Lu et al., 2015):

$$z = C_1\int\zeta^{\frac{-1}{2}}(\zeta-1)^{\frac{-1}{2}}\left(\zeta-\frac{1}{m}\right)^{\frac{-1}{2}}d\zeta + C_2 \tag{42}$$

where, C_1 and C_2 are constants that control the size of rectangle and the location of origin in the z-plane, respectively. C_2 is zero because the origin of the z-plane corresponds to the origin of the ζ-plane. To simplify the solution further, the ζ-plane is transformed onto the τ-plane through the transformation equation $\tau = \zeta^{1/2}$ (Fig. 5), in which case Eq. (42) is given by Lu et al. (2015) as (Table 1):

$$z = \frac{\lambda d}{K(m)}\int\frac{d\tau}{\sqrt{(1-\tau^2)(1-m\tau^2)}} \tag{43}$$

and

$$\tau = sn\left(\frac{zK(m)}{\lambda d}\right) = \frac{sn\left(\frac{xK(m)}{\lambda d}\right)\bar{dn}\left(\frac{yK(m)}{\lambda d}\right)+icn\left(\frac{xK(m)}{\lambda d}\right)dn\left(\frac{xK(m)}{\lambda d}\right)\bar{sn}\left(\frac{yK(m)}{\lambda d}\right)\bar{cn}\left(\frac{yK(m)}{\lambda d}\right)}{\bar{cn}^2\left(\frac{yK(m)}{\lambda d}\right)+msn^2\left(\frac{xK(m)}{\lambda d}\right)\bar{sn}^2\left(\frac{yK(m)}{\lambda d}\right)} = Re^{i\theta} \tag{44}$$

whereλ is the ratio of the aquifer's length to width and *sn*, *cn* and *dn* are standard Jacobi elliptic integrals denoting, respectively, the *sine*, *cosine* and *delta* amplitude elliptic functions; $\bar{sn}\,(y)$ stands for $sn(y, 1-m)$ and similar definitions are made for $\bar{cn}\,(y)$ and $\bar{dn}\,(y)$ (Lu et al., 2015); $R = U^2 + V^2$ and $\theta = tan^{-1}(V/U)$.

The complex potential for a multi-well system in a rectangle aquifer in the τ-plane is:

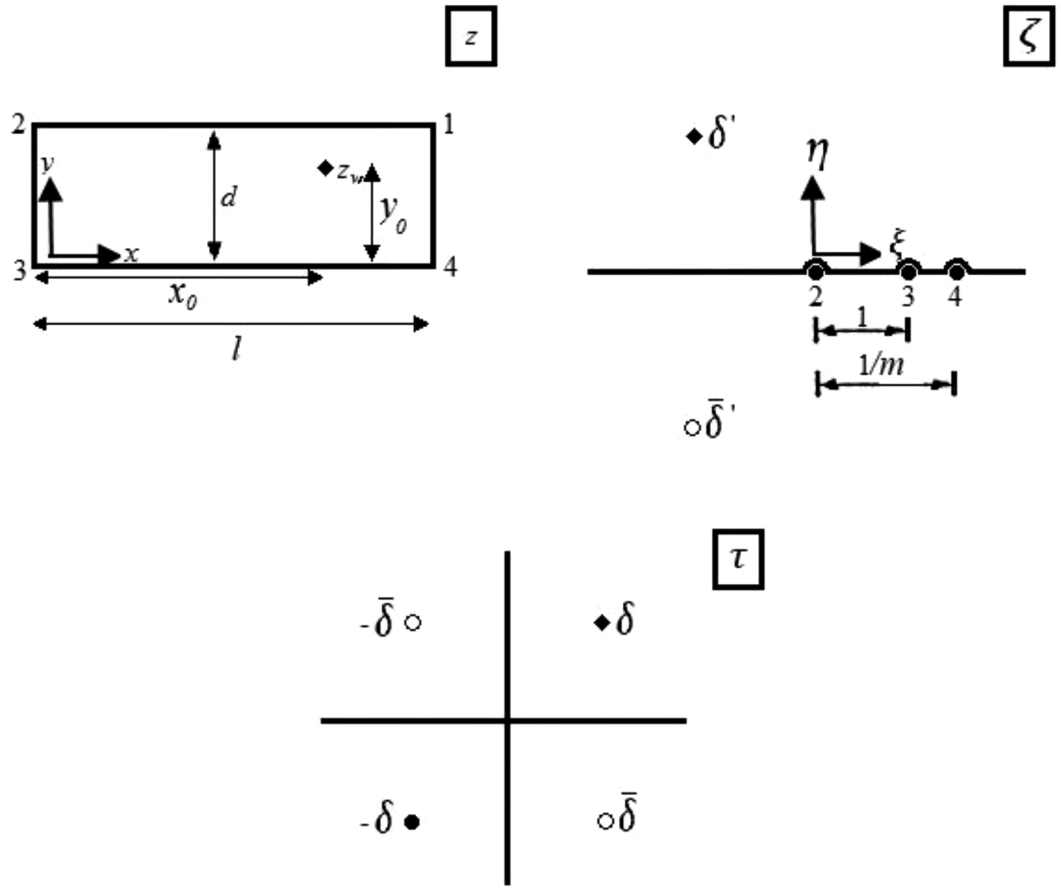

Fig. 5. Mapping the conceptual model from the physical plane (z) to the conformal mapping planes (ζ and τ). Solid circles are the image wells of the same type as the real well (i.e., injection/extraction). δ shows the spatial location of the extraction or injection well in the τ plane and $\bar{\delta}$ is the complex conjugate of δ.

$$\Omega(\tau) = \phi_0 - q_0 \exp(-i\beta)\frac{\lambda d}{K(m)}\int \frac{d\tau}{\sqrt{(1-\tau^2)(1-m\tau^2)}} + \sum_{j=1}^{N} c_j \frac{Q_{wj}}{2\pi}\left\{\ln\left[\frac{(\zeta-\delta_j')(\zeta+\delta_j')}{(\zeta-\bar{\delta}_j')(\zeta+\bar{\delta}_j')}\right]\right\} \quad (45)$$

Eq. (45) can be rewritten in terms of z using Eq. (44):

$$\Omega(z) = \phi_0 - q_0 z \exp(-i\beta) + \sum_{j=1}^{N} c_j \frac{Q_{wj}}{2\pi}\times \left\{\ln\left[\frac{\left(\mathrm{sn}\left(\frac{z\mathrm{K(m)}}{\lambda d}\right)-\mathrm{sn}\left(\frac{z_W\mathrm{K(m)}}{\lambda d}\right)\right)\left(\mathrm{sn}\left(\frac{z\mathrm{K(m)}}{\lambda d}\right)+\mathrm{sn}\left(\frac{z_W\mathrm{K(m)}}{\lambda d}\right)\right)}{\left(\mathrm{sn}\left(\frac{z\mathrm{K(m)}}{\lambda d}\right)-\mathrm{sn}\left(\frac{\bar{z}_W\mathrm{K(m)}}{\lambda d}\right)\right)\left(\mathrm{sn}\left(\frac{z\mathrm{K(m)}}{\lambda d}\right)+\mathrm{sn}\left(\frac{\bar{z}_W\mathrm{K(m)}}{\lambda d}\right)\right)}\right]\right\} \quad (46)$$

where $K(m)$ is the complete elliptic integral. Using the following dimensionless parameters:

$$z_D = \frac{z}{d},\ z_{wDj} = \frac{z_{wj}}{d},\ Q_{wDj} = \frac{Q_{wj}}{Kbd},$$
$$q_{0D} = \frac{q_0}{Kb},\ \Omega_D(z) = \frac{\Omega(z)}{Kbd} \quad (47)$$

Eq. (46) becomes:

$$\Omega_D = \phi_{0D} - q_{0D} z_D \exp(-i\beta) + \sum_{j=1}^{N} c_j \frac{Q_{wDj}}{2\pi}\times \left\{\ln\left[\frac{\left(sn\left(\frac{z_D K(m)}{\lambda}\right)-sn\left(\frac{z_{wD}K(m)}{\lambda}\right)\right)\left(sn\left(\frac{z_D K(m)}{\lambda}\right)+sn\left(\frac{z_{wD}K(m)}{\lambda}\right)\right)}{\left(sn\left(\frac{z_D K(m)}{\lambda}\right)-sn\left(\frac{\bar{z}_{wD}K(m)}{\lambda}\right)\right)\left(sn\left(\frac{z_D K(m)}{\lambda}\right)+sn\left(\frac{\bar{z}_{wD}K(m)}{\lambda}\right)\right)}\right]\right\} \quad (48)$$

The dimensionless discharge potential (ϕ_D) is the real part of Eq. (48) and the imaginary part is the dimensionless stream function (ψ_D):

$$\phi_D = \phi_{0D} - q_{0D}(x_D cos\beta + y_D sin\beta) + \sum_{j=1}^{N} c_j \frac{Q_{wDj}}{4\pi}\times \left\{\ln\frac{[(U_D-U_{wD})^2+(V_D-V_{wD})^2]+[(U_D+U_{wD})^2+(V_D+V_{wD})^2]}{[(U_D-U_{wD})^2+(V_D+V_{wD})^2]+[(U_D+U_{wD})^2+(V_D-V_{wD})^2]}\right\} \quad (49)$$

and

$$\psi_D = -q_{0D}(y_D\cos\beta - x_D\sin\beta) + \sum_{j=1}^{N} c_j \frac{Q_{wDj}}{2\pi}\left[\tan^{-1}\left(\frac{V_D-V_{wD}}{U_D-U_{wD}}\right)+\tan^{-1}\left(\frac{V_D+V_{wD}}{U_D+U_{wD}}\right) - \tan^{-1}\left(\frac{V_D+V_{wD}}{U_D-U_{wD}}\right)-\tan^{-1}\left(\frac{V_D-V_{wD}}{U_D+U_{wD}}\right)\right] \quad (50)$$

As before the first derivative of the discharge potential (Eq. (45)) is set to zero to calculate the stagnation point coordinates, which are then converted to the z-plane using Eq. (44):

$$\frac{d\Omega(\tau)}{d\tau} = -q_0 exp(-i\beta)\frac{\lambda d}{K(m)\sqrt{(1-\tau^2)(1-m\tau^2)}} + \sum_{j=1}^{N} c_j \frac{Q_{wj}}{2\pi}\left[\frac{1}{\zeta-\delta_j}+\frac{1}{\zeta+\delta_j}-\frac{1}{\zeta-\bar{\delta}_j}-\frac{1}{\zeta+\bar{\delta}_j}\right] = 0 \quad (51)$$

Case 4b: In aquifers of irregular/regular shape bounded by more than four boundary segments, the values of C_1, C_2 and a_j in Eq. (41) must be calculated numerically. It is then convenient to compute these unknowns using the Schwarz-Christoffel toolbox in MATLAB as it provides a collection of M-files for the computation and visualization of Schwarz-Christoffel conformal maps (Driscoll and Trefethen, 2002).

The complex potential for a multi-well system in regular/irregular-shaped aquifers in the ζ-plane is:

$$\Omega(\zeta) = \phi_0 - Q_0(\zeta) + \sum_{j=1}^{N} c_j \frac{Q_{wj}}{2\pi}\left[\ln\left(\frac{\zeta-\delta_j}{\zeta-\bar{\delta}_j}\right)\right] \quad (52)$$

where $Q_0(\zeta)$ is the regional flow, which is a function in the ζ-plane that depends on the shape of the aquifer.

To rewrite Eq. (52) in the z-plane, it is solved numerically based on Eq. (41). The real and imaginary parts of the complex potential (Eq. (52)) in the z-plane are the discharge potential and stream function, respectively. They are plotted using dimensionless parameters given in Eq. (3).

To find the positions of the stagnation points, the derivative of the complex potential (Eq. (52)) is calculated with respect to ζ and set equal to zero:

$$\frac{d\Omega(\zeta)}{d\zeta} = -\frac{dQ_0(\zeta)}{d\zeta} + \sum_{j=1}^{N} c_j \frac{Q_{wj}}{2\pi}\left(\frac{1}{\zeta-\delta_j}-\frac{1}{\zeta-\bar{\delta}_j}\right) = 0 \quad (53)$$

The form of the first term in the right-hand side depends on the regional flow functional form in the ζ-plane. The roots of Eq. (53) are the locations of stagnation points in the ζ-plane, and are found numerically using MATLAB. The locations are then easily transformed to the z-plane.

The above results are obtained for confined aquifers with constant saturated thickness. For unconfined aquifers the saturated thickness varies. Eqs. (3), (15), (26), (36), (47) and (52) maybe rewritten to give an approximation for unconfined aquifers by replacing the thickness b with $\bar{h}_0$ (the average saturated thickness) in the dimensionless terms. The derived discharge potential equations can also be rewritten in terms of drawdown (Supplementary Materials).

4. Results and discussion

In the following, the above-presented solutions are used to plot a variety of capture zones. The plotted capture zones delineate the interaction of aquifer-well-boundaries, which are useful for the sustainable management of aquifers in terms of quality and quantity. The effects of the numbers of boundaries or wells, rate and direction of reginal flow and extraction rates on the shape and properties of capture zones are readily investigated. Due to numerous parameters (number, type, location and extraction/injection rates of wells and the rate and direction of regional flow, number of boundary segments) that influence the flow field, many capture envelopes can be simulated.

a) Capture zones of a multi-wells system in a semi-infinite aquifer (Case 1)

The semi-infinite aquifer shown in Fig. 1a is considered for the case of five wells with extraction rates and positions as given in Table 2. We assume that the regional flow rate (dimensionless) and direction are 0.001 and $\pi/2$ rad, respectively. Eqs. (5)–(7) are solved and the equipotential lines, streamlines, stagnation points and the capture envelopes of the five wells are plotted in Fig. 6. In Fig. 6a, the capture envelope of wells 2, 3 and 5 establish a connection with the stream, i.e., the wells are fed by the stream. However, wells 1 and 4 gain their water from the aquifer (which is of infinite extent). In this pumping scenario, if the stream is polluted, wells 2, 3 and 5 will be contaminated. In Fig. 6b, well 3 is assumed to be a wastewater disposal well. In this case, the pattern of the capture envelopes is quite different from that of the first scenario and all extraction wells are contaminated by well 3. These two hypothetical scenarios elucidate the surface and subsurface water interaction in terms of water quality and quantity.

Table 2
Extraction rates and coordinates of wells in Fig. 6.

Fig. 6	Well number	x_{wD}	y_{wD}	Q_{wD}
a, b	1	0.125	0.9	0.01
	2	0.375	0.2	0.02
	3	0.625	0.5	0.03
	4	0.75	0.65	0.01
	5	0.875	0.3	0.02

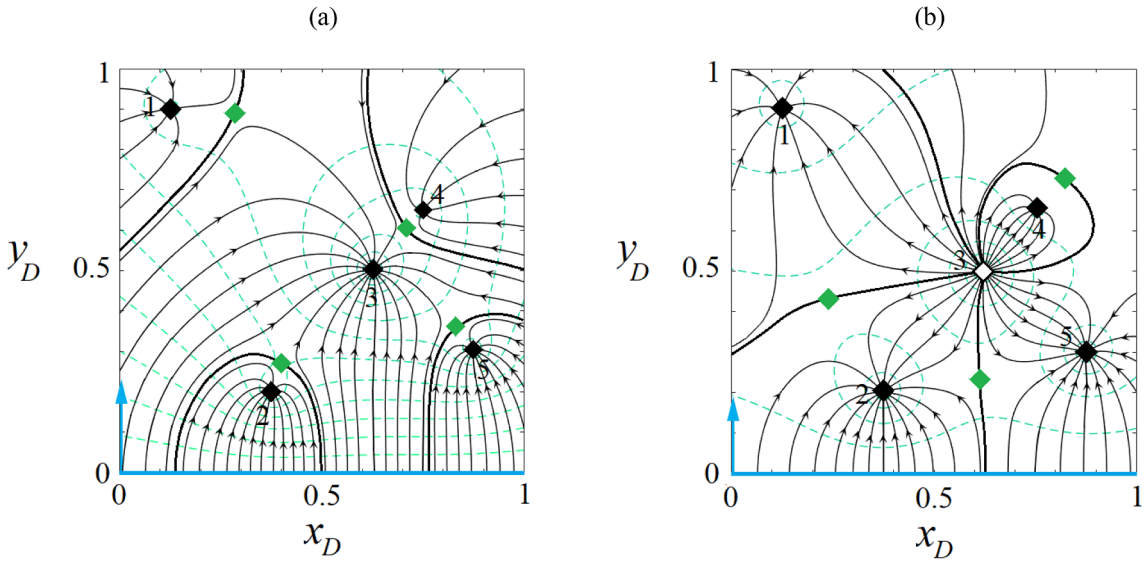

Fig. 6. Capture zone in a semi-infinite aquifer for five extraction/injection wells. In this figure and Figs. 7–11, thick black curves show the limit of the capture envelopes, black thin curves with arrow are streamlines, and green broken lines are equipotential lines. Black, hollow and green diamonds represent the extraction, injection wells and the stagnation points, respectively. The blue arrow illustrates the direction of regional flow. (For interpretation of the references to colour in this figure legend, the reader is referred to the web version of this article.)

b) Capture zones of a multi-wells system in a wedge-shaped aquifer (Case 2)

In this section, a wedge-shaped aquifer that is limited by two intersecting inflow boundaries or two segments of a stream is considered. With the data given in Table 3, Eqs. (17)–(19) are solved for four different scenarios, which are plotted in Fig. 7. Fig. 7 illustrates the potential, streamline, stagnation points and capture envelopes for one, two, three and five wells. In Fig. 7a, the wedge angle and regional flow rate and direction are 0.19π rad, 0.001 and 0.09π rad, respectively. The well captures the regional flow and water gained from the streams.

In Fig. 7b, which considers two pumping wells, the angle between intersecting boundaries is 0.42π rad. There is no regional flow, which causes the equipotential lines to be parallel to the boundaries. A water-line divide is formed between the wells, which are fed by the streams. The capture zone for three wells in a 90°-wedge($\alpha = \pi/2$) with a regional flow direction of $\pi/4$ rad is illustrated in Fig. 7c. Well 1 captures its water from the western boundary. Independently, well 2 receives water from the southern boundary. Well 3, however, shows flow lines to the streams that encompass the capture envelopes of wells 1 and 2. Fig. 7d illustrates the capture zones of five wells in a 127°-wedge-shaped aquifer ($\alpha = 0.7\pi$) without regional flow. The interaction of the aquifer-well-boundary system is self-explanatory in that well 1 is fed by the eastern stream, wells 2 and 3 are fed by the both streams and wells 4 and 5 are supplied by the southern stream. Note that well 3 is also recharged by the infinite boundary.

c) Capture zones of a multi-well system in a peninsula-shaped aquifer (Case 3a)

Here, a peninsula-shaped aquifer is considered. Capture zones for one, two, three and five wells are generated by solving Eqs. (28)–(30) based on the data given in Table 4. A regional flow rate of 0.001 at an angle of $\pi/4$ is assumed. Therefore, the potential along the boundaries is variable.

Fig. 8a depicts the capture zone of a single well. The well is fed by water from the inflow boundaries and the regional flow. Its capture zone covers over half of the aquifer. Fig. 8b illustrates the capture zone of two extraction wells. A water-divide line is formed between the wells and acts as a barrier boundary for well 2. Well 1 captures the regional flow and blocks flow to well 2. As the result, well 2 gains water from the northern and southern streams so that the streamlines of well 2 that are close to the water-divide become parallel to it. In Fig. 8c, where three extraction wells are operating, a water-divide forms and well 3 cannot receive water from the western boundary. Well 1 is fed from the southern and western boundaries, and by capturing the regional flow it prevents any regional flow reaching wells 2 and 3. Well 2 instead receives water from the three boundaries. Fig. 8d shows the capture zones of five extraction wells. Two water-divide lines are formed, one between wells 4 and 5 and another between wells 3 and 4. Well 3 is fed by three boundaries only whereas the others receive water from one or two boundaries. The capture zone of well 4 separates those of wells 3 and 5.

d) Capture zones of multi-well system in triangular aquifers (Case 3b)

Based on Eqs. (38)–(40) and data in Table S1, the capture zones of three wells are plotted for the case of a triangular aquifer. The angles of α_1 and α_2 are 0.37π and0.47π, respectively. In Fig. S2, the case of regional flow of 0.001 at an angle of $\pi/4$ rad is considered. Therefore, the potential along boundaries is variable. Fig. S2 shows that well 1 is mainly supplied by the lower boundary and well 2 is fed by the three boundaries. Although the pumping rate of well 3 is higher than those of other wells, it is not supplied by the boundary along the *y*-axis, but is fully fed by the stream segments in its vicinity. A water-divide line separates the capture envelope of well 3 from that of well 2 and the

Table 3
Extraction rates and coordinates of wells in Fig. 7.

Fig. 7	Well number	x_{wD}	y_{wD}	Q_{wD}
a	1	0.5	0.15	0.01
b	1	0.3	0.2	0.01
	2	0.5	0.7	0.02
c	1	0.3	0.5	0.01
	2	0.5	0.2	0.02
	3	0.7	0.55	0.03
d	1	−0.2	0.7	0.01
	2	0	0.3	0.02
	3	0.2	0.5	0.03
	4	0.4	0.4	0.01
	5	0.7	0.1	0.02

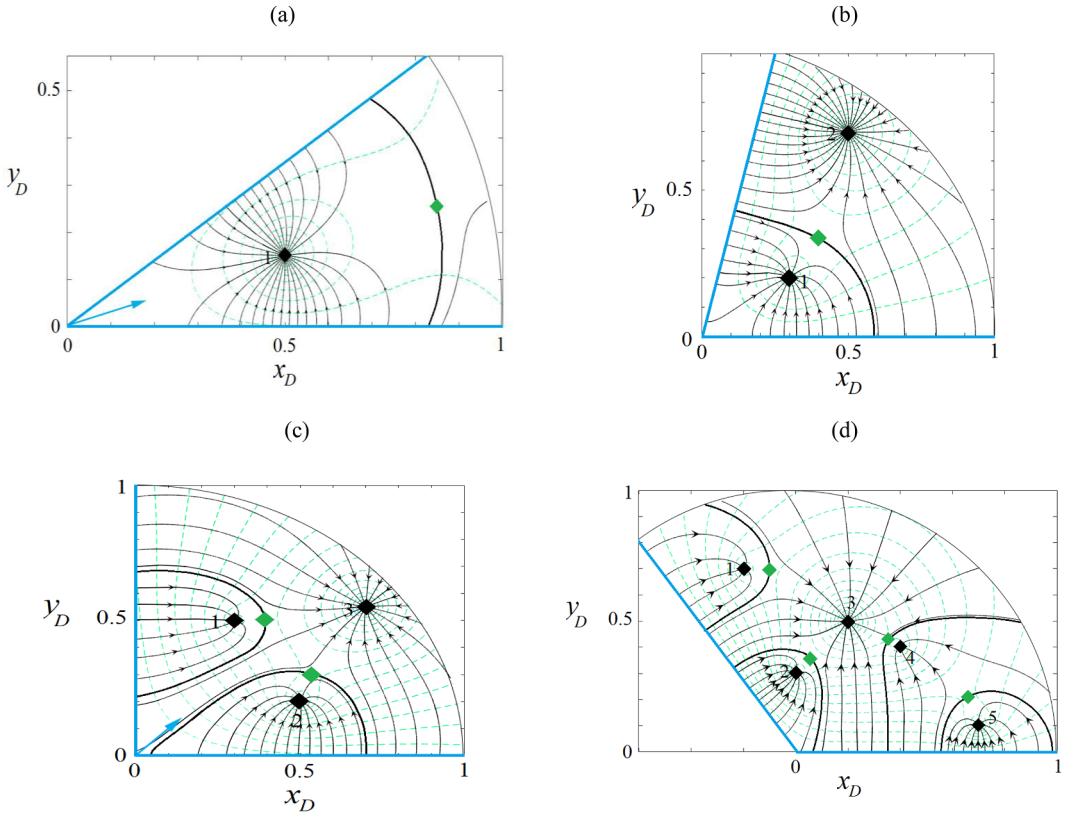

Fig. 7. Capture zones for one (a), two (b), three (c) and five (d) wells in wedged-shaped aquifers.

Table 4
Extraction rates and coordinates of wells in Fig. 8.

Fig. 8	Well number	x_{wD}	y_{wD}	Q_{wD}
a	1	0.5	0.5	0.01
b	1	0.5	0.3	0.01
	2	1.5	0.7	0.02
c	1	0.5	0.25	0.01
	2	1	0.7	0.02
	3	1.5	0.45	0.03
d	1	0.2	0.9	0.01
	2	0.4	0.25	0.02
	3	0.8	0.5	0.03
	4	1.2	0.8	0.01
	5	1.6	0.4	0.02

capture zone of well 2 surrounds that of well 1.

In Fig. 9a, a semi-infinite aquifer with three inflow boundary segments is examined. Five extraction wells are assumed as given in Table 5. The direction of the regional flow is from east to west ($\beta = \pi$). The capture envelopes are calculated based on Eqs. (38)–(40). Except for well 1, the other wells are fed by the inflow boundary. The effect of the regional flow direction is obvious and the capture envelopes trend to the east. If well 1 were a wastewater disposal well, then well 2 would be contaminated only due the low injection rate of well 1 and the direction of the regional flow (Fig. 9b).

e) Capture zones of a multi-wells system in a rectangular aquifer (Case 4a)

In Fig. S3, a rectangle aquifer with four wells is considered. The well coordinates and rates are tabulated in Table S1 and their capture zones are obtained by Eqs. (48) and (49). A regional flow of 0.001 at the direction of $\pi/3$rad is considered. Therefore, the potential along boundaries is variable. In Fig. S3a, the capture zone of well 1 trends in the direction opposite to the regional flow to reach the streams while well 2 is fed by three boundaries and its capture envelope encompasses that of well 1. The capture zone of well 3 is limited by the two water divides formed at the right and left sides of the well. Well 3 prevents regional flow reaching well 4, which is fed by the eastern and northern streams. The aquifer of Fig. S3b is the same as that in Fig. S3a but wells 2 and 3 are injection wells. Well 1 is fed by wells 2 and 3. As a result, if well 2 is a wastewater disposal well it would contaminate well 1 as well as the western, southern and northern boundaries. With the same assumption, injection well 3 contaminates well 1, well 4 and the western, southern and northern streams. Note that well 4 is fully supplied by well 3 and is no longer connected to the boundaries. A closed-loop flow is established between wells 3 and 4, which reflects the usefulness of the derived capture zone models for the entrapment of contaminant plumes that may be exist in the aquifer.

f) Capture zones of a multi-well system in a finite or semi-infinite aquifer bounded by five or more stream segments (Case 4b)

Fig. 10 examines the interaction of aquifer-well-boundary system in an irregularly-shaped aquifers of semi-infinite or finite extent. In Fig. 10a, a semi-infinite aquifer bounded by eight stream segments is pumped by six wells. The extraction rates and positions of the wells are given in Table 6. The rate and direction of the uniform regional flow are 0.001 and$\pi/4$, respectively. Well 1 is supplied by regional flow and has no connection with the stream. In contrast, wells 2 and 3 are fed by the regional flow and by the first, third and last stream segments, respectively. The stream fully supplies wells 5 and 6. The capture envelope of well 4 surrounds the capture envelope of well 2. Well 4 is supplied along the three segments of the stream and along a narrow strip by the regional flow. Fig. 10a is replotted as Fig. 10b by installing an injection well (well 6). The pattern of capture zones changes and wells 3, 4, 5 and 7 are influenced by well 6 while there is no flow between well 6 and wells 1 and 2, although the extent and size of their capture envelopes

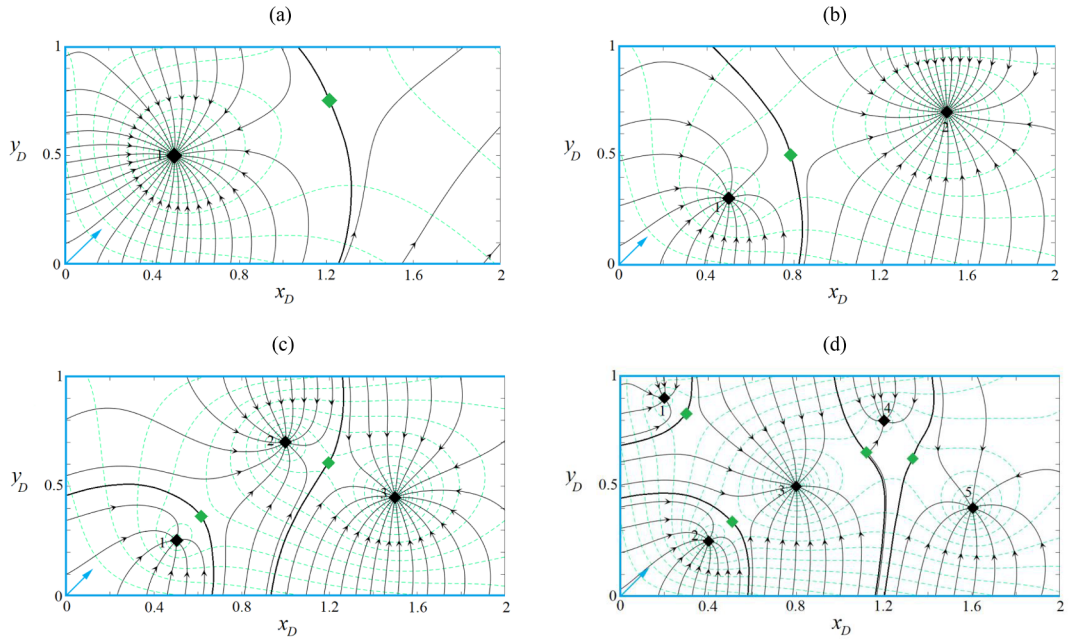

Fig. 8. Capture zones of one (a), two (b), three (c) and five (d) wells in peninsula-shaped aquifers.

are affected indirectly. The so-formed water divide separates the northern and southern portions of the aquifer. Fig. 10c and d are plotted for a finite, irregularly-shaped aquifer (island-aquifer) based on data given in Table 7. The difference between Fig. 10c and d is that in the former case the three wells are extraction wells whereas in Fig. 10d well 1 is an injection well, which recharges the other wells. As the result of the injection well, the capture zone pattern of Fig. 10d changes markedly compared to that of Fig. 10c.

Table 5
Extraction rates and coordinates of extraction wells in Fig. 9.

Well number	x_{wD}	y_{wD}	Q_{wD}
1	0.8	0.5	0.01
2	1	0.8	0.02
3	1	2	0.03
4	2	1.6	0.01
5	2.5	1.8	0.02

5. Validation of the solution

To validate the developed capture zone solutions, the capture zones of Fig. 6a, Fig. 7c and Fig. 9a were generated by MODFLOW 2000 (Harbaugh et al. 2000) and MODPATH (Pollock, 1994) and plotted in Fig. S4. The capture zones and the pattern of streamlines in Fig. S4 generated by the numerical models are comparable to the analytical model capture curves (i.e., Fig. 6a, 7c and 9a). The slight difference is mainly due to the approximation inherent in the numerical models. It is worth mentioning that the usage of the capture zones equations developed in this paper is far easier, more accurate and less time consuming using the abovementioned numerical models, although numerical models are more flexible in dealing with complicated boundary conditions. Fig. S4 demonstrates the credibility of the developed analytical capture zone models and their potential to verify the accuracy of

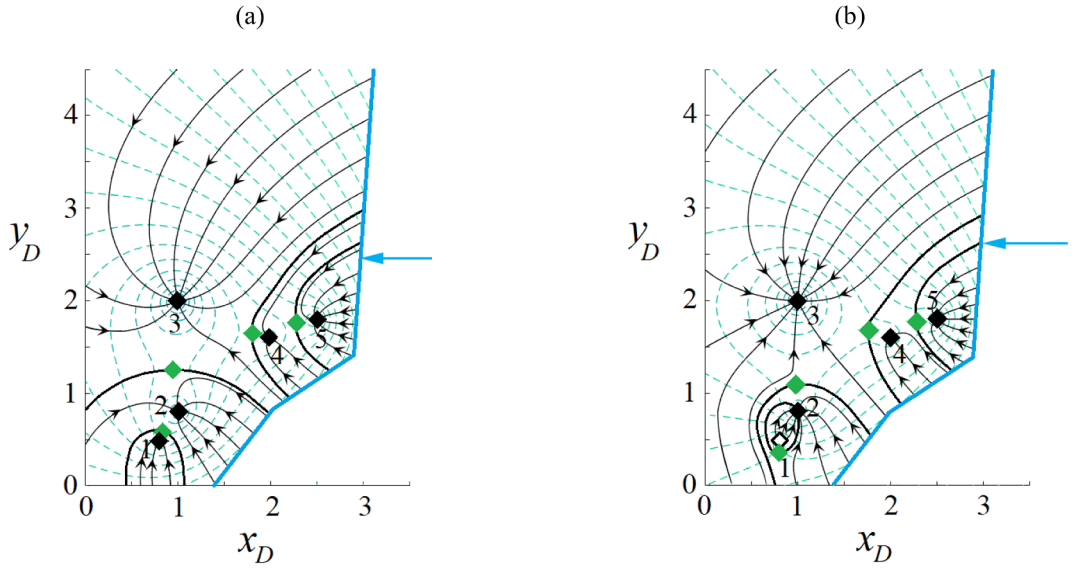

Fig. 9. Capture zones of five wells in a semi-infinite aquifer bounded by three stream segments.

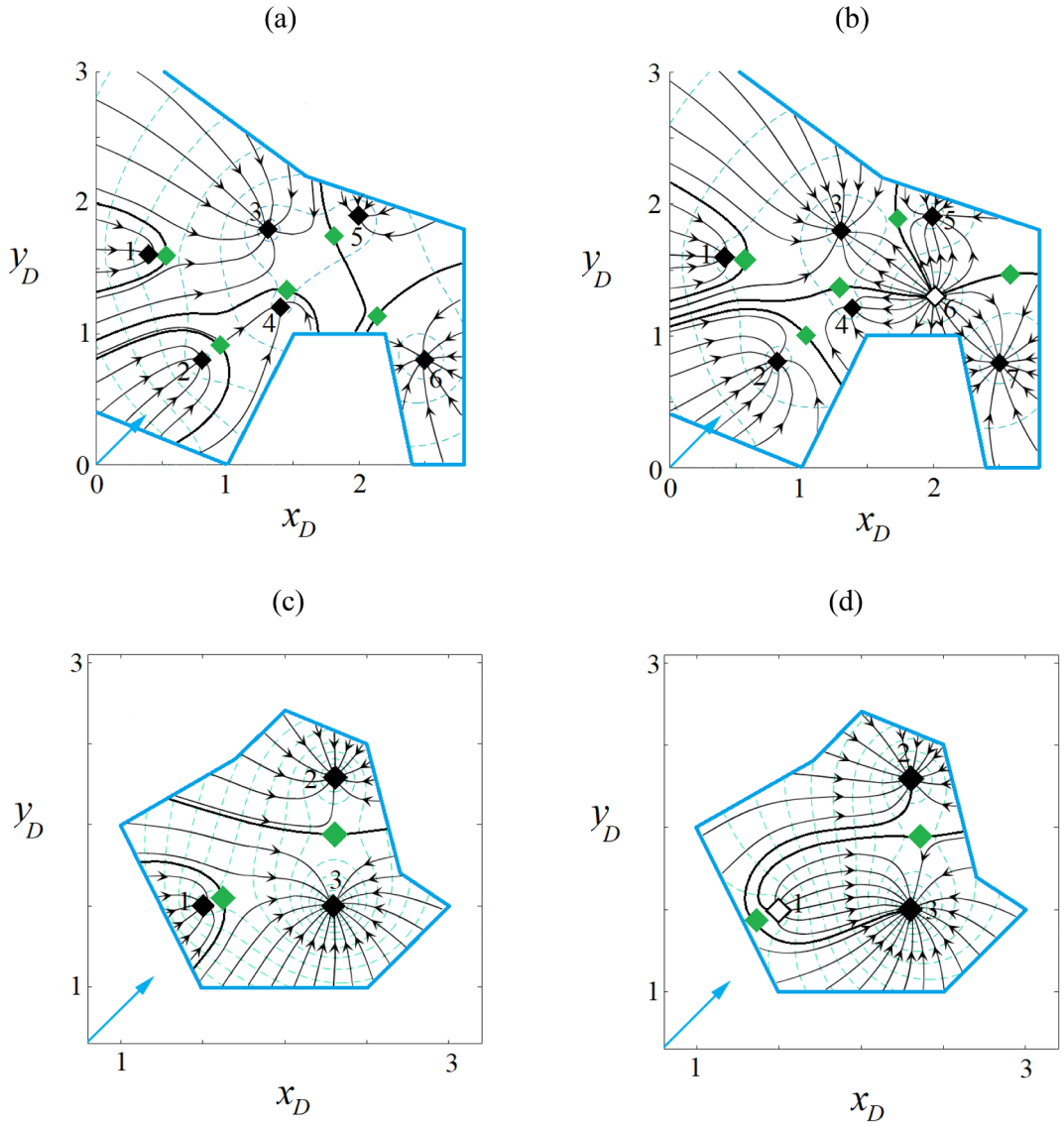

Fig. 10. Capture zones of three wells in semi-infinite (a and b), and finite (c and d) irregular-shaped aquifers.

Table 6
Extraction rates and coordinates of wells in Fig. 10.

Fig. 10	Well number	x_{wD}	y_{wD}	Q_{wD}
a	1	0.4	1.6	0.01
	2	0.8	0.8	0.02
	3	1.3	1.8	0.03
	4	1.4	1.2	0.01
	5	2	1.9	0.02
	6	2.5	0.8	0.03
b	1	0.4	1.6	0.01
	2	0.8	0.8	0.02
	3	1.3	1.8	0.03
	4	1.4	1.2	0.01
	5	2	1.9	0.02
	6	2	1.3	−0.04
	7	2.5	0.8	0.03
c	1	1.5	1.5	0.01
	2	2.3	2.3	0.02
	3	2.3	1.5	0.03
d	1	1.5	1.5	−0.01
	2	2.3	2.3	0.02
	3	2.3	1.5	0.03

numerical models.

6. Groundwater remediation scheme design

The above dimensionless capture zone solutions can be used to design groundwater remediation projects such a bioremediation, pump-and-treat, plume containment, etc. In such projects, polluted groundwater is typically extracted using one or more wells, treated and possibly reinjected. The capture zone, the optimal number of wells, the optimal injection/extraction rates, and the layout of wells with respect to the plume are the main components of an efficient and cost-effective design (Javandel and Tsang, 1986; Zarei-Doudeji and Samani, 2018; Nagheli et al. 2020).

As an example, we consider a semi-infinite aquifer bounded with three stream segments (Fig. 1e). The problem setup includes known dimensions and hydraulic properties as tabulated in Table 7. A contaminant plume is located along the direction of regional groundwater flow (from the east to the west, $\beta = 0$). The aim is to contain the plume hydraulically and prevent its extension downgradient using two or three wells. A logical step is to position one or more extraction wells at the leading edge of the plume and to place an injection well (to inject treated water) in the vicinity of the contaminant source. A solution

Table 7
Aquifer parameter values for Fig. 11.

b (m)	K (m/day)	q_0 (m^2/day)	d (m)			α	
20	5	0.1	2270	1000	3100	127	198

could be determined manually by using Eqs. (38)–(40) to generate a set of capture envelopes for various well layouts and extraction/injection rates. This approach, although cumbersome, could achieve a satisfactory plume capture design. Here, this practice was carried out by embedding Eqs. (38)–(40) within an optimization algorithm, specifically the Genetic Algorithm as presented by Nagheli et al. (2020). The result is presented in Fig. 11 where a closed circulation loop is formed and the optimal plan is achieved, i.e., the plume is contained and can be extracted without disturbing the flow regime of the aquifer. The optimized well positions and extraction/injection rates are given in Table S2.

Another example is illustrated in Fig. S5 where a contaminant plume spreads in the direction of regional flow in a peninsula-shaped aquifer. In Fig. S5a, a set of capture envelopes is plotted for various extraction rates using Eqs. (28) and (29). As can be seen, the capture envelope for $Q_D = 0.005$ fully encompasses the plume, i.e., the well extracts the plume and prevents its spread in the aquifer. However, the capture envelope reaches the stream. An improvement is the duplet well system of Fig. S5b, which forms a closed water circulation loop that separates the plume from the rest of aquifer, and so more efficiently captures the plume than the single-well case presented in Fig. S5a.

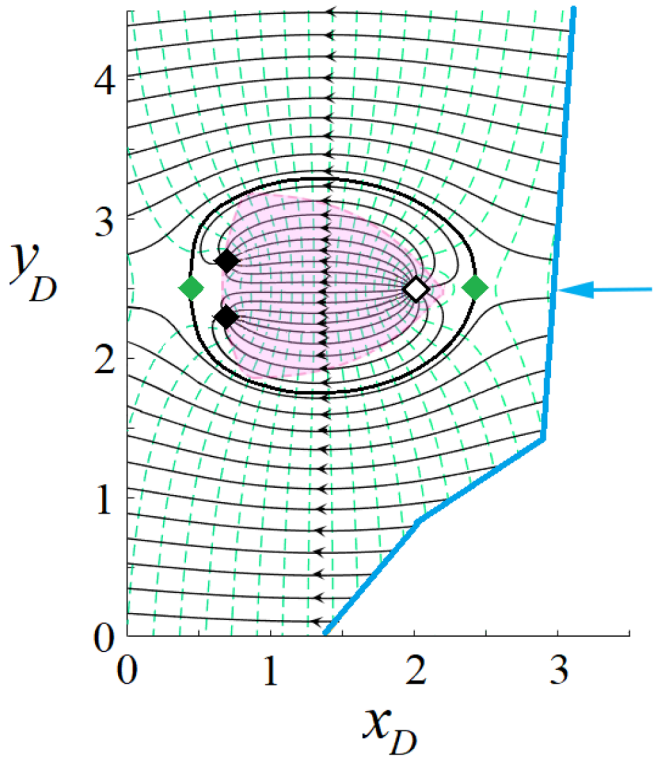

Fig. 11. Groundwater remediation scheme. Solid and hollow diamonds show extraction and injection wells, respectively. The colored area is the original contaminant plume. The thick black line surrounding the plume is the dividing streamline defining the capture zone that separates the plume from the rest of the aquifer.

7. Conclusion

A systematic mathematical formulation for determination of well capture zones consists of the stream function, discharge potential and stagnation points. This work provides this formulation for any number of extraction/injection wells in aquifers bounded by segmented inflow (variable head) boundaries, with/without uniform regional flow. Solutions are obtained based on the theory of complex discharge potentials and the conformal mapping method. The solutions are provided for simple (i.e., one stream segment) to complicated boundary conditions (i.e., n stream segments). The areal extent of the aquifers is semi-infinite or finite and can have regular or irregular shapes. The solutions are provided in dimensionless form.

These solutions generalize existing solutions. The one-stream segment solution is similar to that of Asadi-Aghbolaghi et al. (2011) but our solution generalizes this to consider multiple injection/extraction wells with regional flow in any direction. The two-stream segments solution (i.e., wedge-shaped aquifer), in contrast to Samani and Zarei-Doudeji (2012), is simpler and independent of the wedge angle. The three-stream segments solution is more general and flexible (in terms of the segment interception angles) than the peninsula-shaped aquifers considered by Zarei-Doudeji and Samani (2014). The triangular-aquifers solution is similar to that of Asadi-Aghbolaghi and Seyyedian (2010) but our solution is valid for multiple wells in scalene triangular aquifers. Our rectangular-shaped aquifer solution is independent of the number of wells in contrast to the single-well solution of Lu et al. (2015). The solutions provided for regular and irregular polygonal-shaped aquifers with any number of boundary segments have no comparable existing solutions.

The examples in Figs. 6–11 demonstrate that the size and pattern of the capture envelopes are controlled by the extraction/injection rate, distance of wells from the boundary segments, distances between wells, the rate and direction of regional flow and the initial head along the boundaries. We suggest that the capture zone models presented here can be used as a screening tool for better insight into problems such as surface-subsurface water interaction, water rights adjudication, well head protection plans, issuance of extraction and injection rate permits, quality and quantity management of water resources, etc.

CRediT authorship contribution statement

Setareh Nagheli: Conceptualization, Methodology, Validation, Software. **Nozar Samani:** Conceptualization, Methodology, Supervision, Visualization, Validation, Writing - review & editing, Funding acquisition. **D.A. Barry:** Supervision, Writing - review & editing, Funding acquisition.

Declaration of Competing Interest

The authors declare that they have no known competing financial interests or personal relationships that could have appeared to influence the work reported in this paper.

Acknowledgement

Financial support provided by the Office of Vice Chancellor for Research, Shiraz University (grant no. 95GCU1M1206), Iran is acknowledged. Constructive comments provided by the Editor and anonymous reviewers are appreciated.

Appendix A:. Parameters in Eqs. (27) and (28)

The following terms appear in Eqs. (27) and (28):

$$f_{1D} = \sinh^2(\pi x_D)\cos^2(\pi y_D) + \cosh^2(\pi x_D)\sin^2(\pi y_D)$$

$$f_{2D} = \sinh^2(\pi x_{wjD})\cos^2(\pi y_{wjD}) + \cosh^2(\pi x_{wjD})\sin^2(\pi y_{wjD}) \quad \text{(A1)}$$

$$g_{1D} = 2\sinh(\pi x_D)\cos(\pi y_D)\cosh(\pi x_D)\sin(\pi y_D)$$

$$g_{2D} = 2\sinh(\pi x_{wjD})\cos(\pi y_{wjD})\cosh(\pi x_{wjD})\sin(\pi y_{wjD})$$

Appendix B:. Parameter *m* in Eq. (32)

The derivation of Eq. (32) is based on the observation that, at point 2, z equals di and $\zeta = -1 = \exp(i\pi)$, so that by Eq. (31),

$$di = \frac{C_1 \exp(i\alpha_2)_2F_1\left(\frac{-\alpha_1}{\pi} + 1, \frac{\alpha_2}{\pi}; \frac{\alpha_2}{\pi} + 1; 1\right)}{\frac{\alpha_2}{\pi}} \quad \text{(B1)}$$

and

$$C_1 = \frac{\alpha_2 di}{\pi \exp(i\alpha_2)_2F_1\left(\frac{-\alpha_1}{\pi} + 1, \frac{\alpha_2}{\pi}; \frac{\alpha_2}{\pi} + 1; 1\right)} \quad \text{(B2)}$$

In Eq. (32), $m = C_1$ as written here.

Appendix C. Supplementary data

Supplementary data to this article can be found online at https://doi.org/10.1016/j.hydroa.2020.100053.

References

Ahlfeld, D.P., Sawyer, C.S., 1990. Well location in capture zone design using simulation and optimization techniques. Groundwater 28 (4), 507–512. https://doi.org/10.1111/j.1745-6584.1990.tb01705.x.

Asadi-Aghbolaghi, M., Seyyedian, H., 2010. An analytical solution for groundwater flow to a vertical well in a triangle-shaped aquifer. J. Hydrol. 393 (3–4), 341–348. https://doi.org/10.1016/j.jhydrol.2010.08.034.

Asadi-Aghbolaghi, M., Rakhshandehroo, G.R., Kompani-Zare, M., 2011. Analytical solutions for the capture zone of a pumping well near a stream. Hydrogeol. J. 19, 1161–1168. https://doi.org/10.1007/s10040-011-0741-2.

Asadi-Aghbolaghi, M., Rakhshandehroo, G.R., Kompani-Zare, M., 2013. An analytical approach to capture zone delineation for a well near a stream with a leaky layer. Hydrolog. Sci. J. 58 (8), 1813–1823.

Bair, E.S., Roadcap, G.S., 1992. Comparison of flow models used to delineate capture zones of wells: 1. Leaky-confined fractured-carbonate aquifer. Groundwater 30 (2), 199–211. https://doi.org/10.1111/j.1745-6584.1992.tb01792.x.

Bear, J., 1979. Dynamics of Fluids in Porous Media. Dover Publications Inc., New York.

Bear, J., 1972. Dynamics of Fluids in Porous Media. American Elsevier, New York pp. 125–129.

Christ, J.A., Goltz, M.N., 2002. Hydraulic containment: analytical and semi-analytical models for capture zone curve delineation. J. Hydrol. 262 (1–4), 224–244. https://doi.org/10.1016/S0022-1694(02)00026-4.

Driscoll, T.A., Trefethen, L.N., 2002. Schwarz-Christoffel Mapping. Cambridge University Press, UK.

Faybishenko, B.A., Javandel, I., Witherspoon, P.A., 1995. Hydrodynamics of the capture zone of a partially penetrating well in a confined aquifer. Water Resour. Res. 31 (4), 859–866. https://doi.org/10.1029/94WR02707.

Ferris, J., Knowles, D., Brown, R., Stallman, R., 1962. Theory of aquifer tests. Geol. Surv. Water-Supply Pap. 1536-E, 69–174. https://doi.org/10.3133/wsp1536E.

Fienen, M.N., Luo, J., Kitanidis, P.K., 2005. Semi-analytical homogeneous anisotropic capture zone delineation. J. Hydrol. 312 (1–4), 39–50. https://doi.org/10.1016/j.jhydrol.2005.02.008.

Gailey, R.M., Gorelick, S.M., 1993. Design of optimal, reliable plume capture schemes: application to the Gloucester landfill ground-water contamination problem. Groundwater 31 (1), 107–114. https://doi.org/10.1111/j.1745-6584.1993.tb00834.x.

Grubb, S., 1993. Analytical model for estimation of steady-state capture zones of pumping wells in confined and unconfined aquifers. Groundwater 31 (1), 27–32. https://doi.org/10.1111/j.1745-6584.1993.tb00824.x.

Harbaugh, A.W., Banta, E.R., Hill, M.C., McDonald, M.G., 2000. MODFLOW-2000, the U. S. Geological Survey Modular Ground-Water Model-User Guide to Modularization Concepts and the Ground-Water Flow Process. Open-file Report. U. S. Geological Survey (92) 134.

Huang, C.S., Yeh, H.D., 2015. Estimating stream filtration from a meandering stream under the Robin condition. Water Resour. Res. 51 (6), 4848–4857. https://doi.org/10.1002/2015WR016975.

Huang, C.-S., Yeh, H.-D., 2016. An analytical approach for the simulation of flow in a heterogeneous confined aquifer with a parameter zonation structure. Water Resour. Res. 52 (11), 9201–9212. https://doi.org/10.1002/2016WR019443.

Intaraprasong, T., Zhan, H., 2007. Capture zone between two streams. J. Hydrol. 338, 297–307. https://doi.org/10.1016/j.jhydrol.2007.03.005.

Javandel, I., Doughty, C., Tsang, C., 1984. Groundwater transport, Handbook of Mathematical Models. Water Resour. Monogr 10 American Geophysical Union, Washington DC.

Javandel, I., Tsang, C., 1986. Capture-zone type curves: a tool for aquifer cleanup. Groundwater 24 (5), 616–625. https://doi.org/10.1111/j.1745-6584.1986.tb03710.x.

Lu, C., Xin, P., Li, L., Luo, J., 2015. Steady state analytical solutions for pumping in a fully bounded rectangular aquifer. Water Resour. Res. 51, 8294–8302. https://doi.org/10.1002/2015WR017019.

Luo, J., Kitanidis, P.K., 2004. Fluid residence times within a recirculation zone created by an extraction-injection well pair. J. Hydrol. 295 (1–4), 149–162. https://doi.org/10.1016/j.jhydrol.2004.03.006.

Muskat, M., 1946. The flow of homogeneous fluids through porous media. In: Edwards, J. W. (Ed.), Ann Arbor, USA 306 T.

Nagheli, S., Samani, N., Barry, D.A., 2020. Multi-well capture zones in strip-shaped aquifers. PLOS ONE. https://doi.org/10.1371/journal.pone.0229767.

Pollock D.W., 1994. User's Guide for MODPATH/MODPATH-PLOT, Version 3: A particle tracking post-processing package for MODFLOW, the U. S. Geological Survey finite-difference ground-water flow mode, the US Geol. Survey, Open- File Report 94-464.

Samani, N., Zarei-Doudeji, S., 2012. Capture zone of a multi-well system in confined and unconfined wedge-shaped aquifers. Adv. Water Resour. 39, 71–84. https://doi.org/10.1016/j.advwatres.2012.01.004.

Schafer, D., 1996. Determining 3D capture zones in homogeneous, anisotropic aquifers. Groundwater 34, 628–639. https://doi.org/10.1111/j.1745-6584.1996.tb02050.x.

Shan, C., 1999. An analytical solution for the capture zone of two arbitrarily located wells. J. Hydrol. 222, 123–128. https://doi.org/10.1016/S0022-1694(99)00101-8.

Springer, A.E., Bair, E.S., 1992. Comparison of methods used to delineate capture zones of wells: 2. Stratified-drift buried-valley aquifer. Groundwater 30 (6). https://doi.org/10.1111/j.1745-6584.1992.tb01574.x.

Strack, O.D.L., 1989. Groundwater Mechanics. Prentice Hall, New Jersey.

Taylor, J.Z., Person, M., 1998. Capture zone delineations on island aquifer systems. Groundwater 36, 722–730. https://doi.org/10.1111/j.1745-6584.1998.tb02189.x.

Tiedeman, C., Gorelick, S.M., 1993. Analysis of uncertainty in optimal groundwater contaminant capture design. Water Resour. Res. 29 (7), 2139–2153. https://doi.org/10.1029/93WR00546.

Todd, D.K., Mays, M.M., 2005. Groundwater Hydrology. John Wiley & Son Inc, New Jersey.

Voss, C.I., 1984. A finite-element simulation model for saturated-unsaturated, fluid-density-dependent ground-water flow with energy transport or chemically-reactive single-species solute transport, U.S. Geological Survey, Water-Resources Investigations Report 84-4369. https://doi.org/10.3133/wri844369.

Wilson, J.L., 1993. Induced infiltration in aquifers with ambient flow. Water Resour. Res. 29 (10). https://doi.org/10.1029/93WR01393.

Xia, Q., Kuang, X.X., Zhan, H.B., Xu, M., Wang, S.Y., Fan, S., 2020. Analytical solution of capture time to a partially penetrating well in a semi-infinite aquifer. J. Hydrol. 580, 124233.

Zarei-Doudeji, S., Samani, N., 2018. Capture zone of a multi-well system in bounded

rectangular-shaped aquifers: modeling and application. Iran. J. Sci. Technol. Trans. A Sci. 42, 191–201. https://doi.org/10.1007/s40995-016-0046-3.
Zarei-Doudeji, S., Samani, N., 2014. Capture zone of a multi-well system in bounded peninsula-shaped aquifers. J. Contam. Hydrol. 164, 114–124. https://doi.org/10.1016/j.jconhyd.2014.05.015.
Zhan, H., Cao, J., 2000. Analytical and semi-analytical solutions of horizontal well capture times under no-flow and constant-head boundaries. Adv. Water Resour. 23 (8), 835–848. https://doi.org/10.1016/S0309-1708(00)00014-2.
Zhan, H.B., Zlotnik, V.A., 2002. Ground water flow to horizontal and slanted wells in unconfined aquifers. Water Resour. Res. 38 (7), 1108. https://doi.org/10.1029/2001WR000401.
Zlotnik, V.A., 1997. Effects of anisotropy on the capture zone of a partially penetrating well. Groundwater 35, 842–847. https://doi.org/10.1111/j.1745-6584.1997.tb00152.x.